Low-Frequency Electro-Magnetic Stirring during AC TIG Welding of AA6082

Master's Thesis

C.H.J. Gerritsen

Delft University of Technology
Laboratory of Materials Science
Rotterdamseweg 137
2628 AL Delft
The Netherlands

March 1999

Supervisor: Dr.ir. M.J.M. Hermans
Professor: Prof.dr. G. den Ouden

Abstract

In this report, some effects of low-frequency (0 - 10 Hz) Electro-Magnetic Stirring (EMS) during Alternating Current (AC) Tungsten Inert Gas (TIG) welding are described. With EMS, rotational weld pool flow is induced through Lorentz interaction ($\vec{F}_L = \vec{B} \times \vec{j}$) between an external magnetic field and the welding current. The main target is to influence weld metal solidification through changes in the temperature gradients, increased constitutional supercooling and supply of nuclei. Possible results are grain refinement and a changed texture, and thereby improved weld properties.

The material used in this project was AA6082 aluminium-magnesium-silicon alloy. This alloy is known to be susceptible to hot cracking (solidification cracking). Therefore, next to improving the grain structure, another point of attention was the possibility of diminishing this hot-cracking susceptibility solely through application of EMS (i.e. no filler wire was used).

EMS is most effective with alternating axial magnetic fields (i.e. the magnetic field lines (anti)parallel to the electrode axis). To reach alternating stirring action, commonly either the magnetic field or the welding current is alternated at the desired stirring frequency. However, aluminium is generally welded with alternating welding current with a frequency of 50 Hz to break down the oxide layer on the weld pool. This project evaluated the possibility to stir at a chosen low frequency, while welding with a welding current alternating at 50 Hz. To reach this, an alternating magnetic field should be applied with the frequency equal to the desired stirring frequency plus the frequency of the alternating welding current. Under these conditions, low-frequency components arise, which induce low-frequency stirring, whilst the high-frequency components are too fast for the fluid to follow, due to its inertia.

This project has shown that it is indeed effective to apply low-frequency EMS during AC TIG welding in this way.

Improvement of the grain structure through grain refinement as well as a change in texture was found to play a role at low travel speeds (<4 mm/s) in particular. Grain refinement was not a result of an increased number of nuclei, but was caused by periodical changes in the temperature gradients. As a result of these changes, grains are

hindered in their growth, allowing new grains to be formed. This mechanism was particularly effective at high stirring frequencies (~10 Hz). Changes in texture were mainly found at low stirring frequencies (1 - 2 Hz), and also resulted from changes in temperature gradient. These changes in texture may be effective to diminish the hot-cracking susceptibility, as they force the hot crack to periodically alter its direction, dissipating energy.

At a higher travel speed (8 mm/s), the effect of EMS was rather worsening the grain structure than improving it. Due to the lower G/R ratio at this travel speed, finer grains are already formed without EMS. However, the additional application of EMS introduced zones with columnar grains.

Other effects of EMS are an increased weld penetration and weld width and the introduction of large gas bubbles. The preliminary hot-cracking tests showed little effect of the grain structure of stirred welds on the hot-cracking susceptibility.

Samenvatting

In dit verslag worden enkele effecten van laagfrequent (0 - 10 Hz) Elektro-Magnetisch Roeren (EMS) gedurende wisselstroom (AC) TIG-lassen beschreven. Met EMS wordt rondgaande lasbadstroming opgewekt door Lorentz-interactie ($\vec{F}_L = \vec{B} \times \vec{j}$) tussen een extern magneetveld en de lasstroom. Het hoofddoel hiervan is beïnvloeding van de korrelstructuur van het lasmetaal door veranderingen in de temperatuurgradiënten, door toenemende constitutionele onderkoeling en door toename van het aantal nucleï. Mogelijke resultaten zijn korrelverfijning en een veranderde textuur, en daardoor verbeterde eigenschappen.

Het materiaal dat gebruikt is in dit project was de AA6082 aluminium-magnesium-silicium legering. Het is bekend dat deze legering gevoelig is voor warmscheuren (stolscheuren). Daarom was naast het verbeteren van de korrelstructuur een aandachtspunt het verminderen van deze scheurgevoeligheid, en wel door middel van EMS alleen (dat wil zeggen zonder het gebruik van toevoegmateriaal).

EMS is het effectiefst als het wordt toegepast met een wisselend, axiaal magneetveld (dat wil zeggen de veldlijnen (anti)parallel aan de electrode). Om wisselend roeren te bewerkstelligen wordt gewoonlijk een wisselend magneetveld, danwel een wisselstroom gebruikt. Aluminium wordt evenwel gewoonlijk gelast met wisselstroom met een frequentie van 50 Hz, om de op het lasbad aanwezige oxidehuid te doorbreken. In dit project is de mogelijkheid onderzocht om met een bepaalde frequentie te roeren, terwijl toch met 50 Hz wisselstroom wordt gelast. Om dit te bereiken, dient een wisselend magneetveld te worden gebruikt met een frequentie gelijk aan de gewenste roerfrequentie plus de frequentie van de wisselstroom. In dat geval treden laagfrequente zwevingen op die het roeren bewerkstelligen, terwijl de hoogfrequente componenten te snel zijn om door de lasbadstroming gevolgd te worden, gezien de traagheid van het gesmolten metaal.

Dit project heeft laten zien dat het inderdaad mogelijk is om op dergelijke wijze laagfrequente EMS toe te passen tijdens AC TIG-lassen.

Het is gebleken dat verbetering van de korrelstructuur, zowel door korrelverfijning als door een verandering in textuur, voornamelijk een rol speelt bij lage

voortloopsnelheden (<4 mm/s). De korrelverfijning is niet het resultaat van een toegenomen hoeveelheid nucleï, maar van de periodieke veranderingen in de temperatuurgradiënten. Als gevolg hiervan worden korrels gehinderd in hun groei, waardoor nieuwe korrels kunnen ontstaan. Dit mechanisme is vooral effectief bij hoge frequenties (~10 Hz). Veranderingen in textuur werden hoofdzakelijk gevonden voor lage roerfrequenties (1 - 2 Hz), en ook deze waren het gevolg van veranderingen in temperatuurgradiënt. De textuurveranderingen kunnen mogelijkerwijs bijdragen aan het verminderen van de warmscheurgevoeligheid, aangezien zij de scheur dwingen perodiek van richting te veranderen, waarbij energie wordt gedissipieerd.

Bij hogere voortloopsnelheden (8 mm/s) heeft EMS eerder een averechts effect dan dat het voor verbetering zorgt. Ten gevolge van de lage G/R-ratio bij deze voortloopsnelheid worden fijne korrels al gevormd zonder EMS, terwijl EMS zones met kolomvormige kristallen introduceerde.

Andere effecten van EMS zijn een toename in doorlassing en lasbreedte en het invangen van gasbellen. Inleidende warmscheurproeven toonden weinig effect van een geroerde structuur op de warmscheurgevoeligheid.

Table of contents

Nomenclature

A	weld pool cross section area	$[m^2]$
B	magnitude of the magnetic induction (magnetic field strength)	[T]
dV	volume element	$[m^3]$
F_L	magnitude of the Lorentz force	[N]
g_z	gravitational acceleration	$[m/s^2]$
G	temperature gradient	[K/m]
HI	heat input	[J/m]
I	welding current	[A]
j	magnitude of the current density	$[A/m^2]$
m	summation index	[-]
n	summation index	[-]
P	pressure	[Pa]
q	amount of heat needed per unit volume to heat the weld metal from room temperature to the melting temperature and to melt it	$[J/m^3]$
r	weld pool radius	[m]
R	speed of the solidification front	[m/s]
SQ	stirring quotient	[1/m]
t	time	[s]
T	temperature	[K]
T_a	actual temperature ahead of the solidification front	[K]
T_L	liquidus temperature	[K]
U	welding voltage	[V]
v	travel speed	[m/s]
x	variable	[-]
X_L	increased alloying concentration ahead of the solidification front	[%]
y	variable	[-]
α	smallest angle between the current density vector and the magnetic induction	[°]
β	thermal expansion coefficient	$[m^3/K]$
η	viscosity	$[N \cdot s/m^2]$
η_s	melting efficiency	[%]

η_p	process efficiency	[-]
ϑ	angle between the welding direction and the solidification direction	[°]
ν	frequency	[Hz]
ν_S	stirring frequency	[Hz]
ρ	density	[kg/m^3]
ϕ	phase difference	[-]
∇	nabla operator: $(\frac{\partial}{\partial x}+\frac{\partial}{\partial y}+\frac{\partial}{\partial z})$, used to calculate the gradient in the x-, y- and z-direction	

Frequently used indexes:

r	in radial direction
θ	in azimuthal direction
z	in axial direction
j	of the current density
B	of the magnetic induction
$\bar{}$	over a symbol denotes a vector

1. Introduction

Most aluminium alloys have attractive properties for constructional applications, such as a high strength-to-weight ratio and a good corrosion resistance. However, some of these are affected by welding. As the grain structure of the weld metal is decisive for its properties, many investigations aim at improving it. This can be reached by influencing the weld pool behaviour and thereby the solidification of the weld metal.

In this project a study was made of some effects of low-frequency Electro-Magnetic Stirring (EMS) during Alternating Current (AC) TIG welding of AA6082 aluminium-magnesium-silicon alloy. Particular interest was on the potentially grain refining effect of EMS. Furthermore, some attention was given to diminishing the hot-cracking susceptibility of the alloy without changing its chemical composition (i.e. no filler wire addition during welding), but through changing the primary grain structure alone. Two possible effects of EMS are then used: grain refinement and weaving of the centreline. The main parameters were the travel speed and the stirring frequency.

Although already a considerable amount of research has been performed on EMS (cf. [1]), only little research has been performed with both the welding current and the magnetic field alternating at frequencies of around 50 Hz [2]. However, in this way, due to low-frequency components, low-frequency EMS (order of 0.1 to 10 Hz) can be applied, whilst maintaining the surface cleaning action of the alternating welding current, necessary for welding aluminium.

The outline of this report is as follows. Chapter 2 starts with a general description of the arc welding process. It includes characteristics of and phenomena occurring in the electric arc and in the weld pool. Of course special attention is given to the solidification of weld metal. In Chapter 3, the theoretical background of EMS is presented as well as a discussion of its possible effects. Chapter 4 describes the experimental set-up, calibration and procedures. The results are presented and discussed in Chapter 5. The last chapter presents some conclusive remarks and recommendations for future research.

This report was written as a Master's Thesis in the framework of a six-month graduation project to gain the title of "ingenieur" (cp. M.Sc.) in Materials Science and Engineering at Delft University of Technology. The project has been performed within the Welding and Non-Destructive Testing Section of the Laboratory for Materials Science, part of the Department of Applied Sciences.

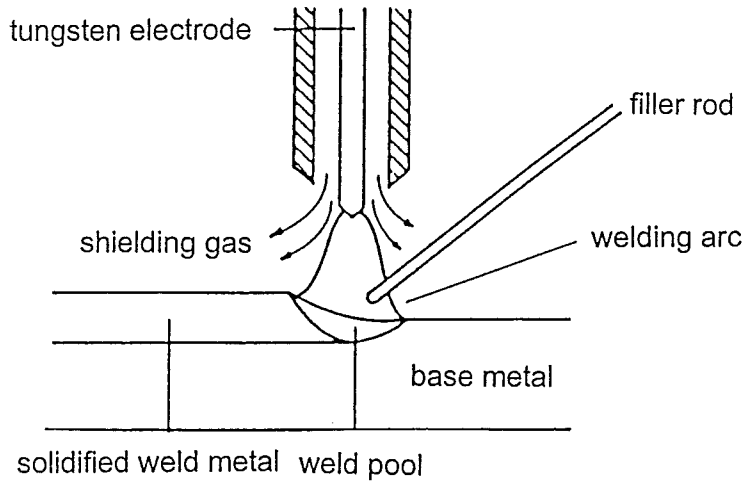

Figure 2.1 Schematic representation of the set-up for TIG welding [3].

2. A general description of arc welding and of weld metal solidification

2.1. Introduction

Arc welding is a metals joining technique in which the joint is heated by a stable electric arc struck between the metallic workpiece and an electrode. By moving the electrode (and thereby the arc) along the workpiece, the metal is melted along the joint line. After the arc has passed, the liquid metal solidifies again, forming a continuous joint.

A very common arc welding technique is Tungsten Inert Gas (TIG) welding (also known as Gas Tungsten Arc Welding, GTAW). Because of its well-defined, stable arc, TIG welding is particularly suitable for high-precision welding of small objects and for welding sheet material. It is also frequently used to deposit the root weld in the case of a multi-pass weld. If necessary, for instance to fill up grooves, filler metal can be added to the weld pool. Some disadvantages of TIG welding are its poor penetration, its sensitivity to small variations in the composition of the base material and its relatively low travel speed.

The following section discusses TIG welding in general. In Section 2.3 and 2.4 the welding arc and weld pool are discussed, respectively. Most importantly, the last section discusses the solidification of weld metal.

2.2. Tungsten Inert Gas welding

A schematic representation of the set-up for the TIG welding process is given in Figure 2.1 [3]. The electric welding arc is struck between the non-consumable tungsten electrode and the workpiece. The workpiece metal is heated and partially melted by the energy supplied by the electric arc. The molten metal is called the weld pool and it is protected, as is the electrode, from environmental influences (e.g. oxidation) by a shielding gas (generally argon, helium or a mixture of both).

To ignite the arc, several techniques can be used. The essence of all these techniques is the same: to stimulate emission of electrons from the cathode. The most commonly used technique superimposes a high-frequency high-voltage on the arc

voltage used. In this way, no contact is made between the sample and the (non-melting!) electrode, preventing contamination of either. In this project, however, the arc was ignited by short-circuiting the electrode and the workpiece with a carbon stick. This was done to prevent interference of the high-frequency voltage with electrical equipment, for instance the computer controlling the magnetic field.

In general, to transfer most of the generated heat to the workpiece and to prevent the tungsten electrode from melting, direct current is used with negative polarity of the electrode (DCEN). Because the electrode is then used as the electron emitter (cathode), it is cooled down by the energy needed for emission of electrons (i.e. work function).

However, for aluminium it is somewhat more complex. TIG welding of aluminium with an argon gas shielding cannot be accomplished with the electrode as the cathode, because an impenetrable oxide layer is present on the weld pool surface, isolating the weld pool. Although this layer can be broken down by ion bombardment, this would require the workpiece to be charged negative, causing the positively-poled electrode to melt. Therefore, alternating current is applied, to prevent the electrode from melting in the one half cycle, and to break down the oxide layer in the other. (It should be noted that with helium as shielding gas, aluminium can be welded with direct current, because of the much higher temperature of the arc. This higher temperature disturbs the oxide layer, allowing the electrode to be poled negatively. However, helium is much more expensive and therefore the use of alternating current with an argon shielding is more common.)

The next section discusses some general properties of the welding arc.

2.3. The welding arc

The welding arc, which conducts the electric current between the cathode and the anode, consists of electrons, ions and gas molecules originating from the electrode, from the shielding gas and from the workpiece. In order to maintain a stable arc, a high current and a low voltage are used, creating an electric power U•I per unit time, with U the arc voltage (V) and I the welding current (A). The arc is generally bell-shaped, although its exact shape and size are dependent on the shape of the electrode, on the flow of the shielding gas and on the length of the arc. The highest temperature (which can be as high as 18.000 K) in a normal arc column is found on the axis close to the cathode,

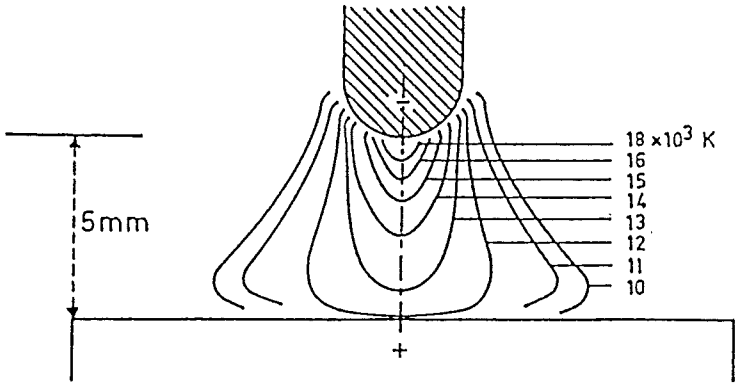

Figure 2.2 Temperature distribution in a 200A arc between a tungsten electrode and a water-cooled copper anode. Argon shielding. [3].

where the arc is narrowest. The temperature decreases along this axis, as the arc broadens, and in radial outward direction (Figure 2.2 [3]).

Inside the arc, various physical phenomena occur: ionisation, dissociation, electrical conduction, heat conduction, radiation and plasma convection. The two phenomena of most importance to our subject - electrical conduction and plasma convection - are now briefly discussed.

Probably the most important of the two is the electrical conductivity of the welding arc. The total electric current in the arc column equals the sum of the electron current from cathode to anode and the ion current from anode to cathode. (In practice, however, the ion current is negligible in comparison to the electron current.) The electric current gives rise to an indigenous magnetic field, while the arc itself, as an electric conductor, is susceptible to magnetic fields. This can result in weld irregularities and defects, as well as in arc blow, extinguishing the arc.

Plasma convection - the second phenomenon of importance - results from gradients in the arc pressure. These pressure gradients arise due to two mechanisms. Firstly, a pressure gradient results from the interaction between the indigenous magnetic field and the electric current. This interaction results in an inward directed Lorentz force, contracting the arc and thereby increasing the arc pressure. However, as the current inevitably diverges in the arc, a gradient in the Lorentz force exists. As a consequence, a pressure gradient is formed, causing plasma flow (plasma jet) along this pressure gradient. The plasma jet can reach considerable velocities of up to 200 m/s [3]. Secondly, a pressure gradient is formed due to differences in plasma density, which in turn are caused by differences in temperature.

2.4. The weld pool

The heat transferred to the workpiece melts some of the metal, thus creating the weld pool. The molten metal solidifies again at the back of the pool, after the arc has passed. The dimensions and the geometry of the weld pool play an important role with regard to the final structure of the weld metal. Therefore, in this section, some influential parameters are discussed, such as the heat input, the travel speed and the fluid flow inside the weld pool.

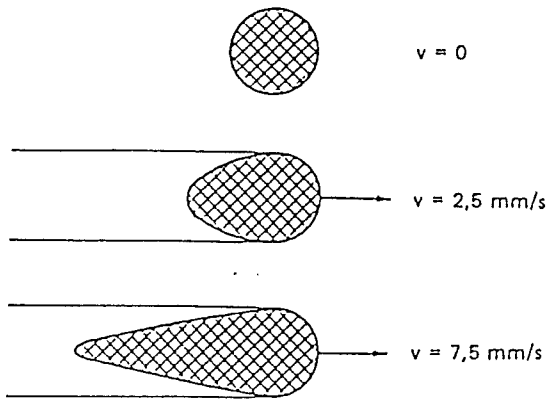

Figure 2.3 Schematic examples of the weld pool shape for different values of the travel speed [3].

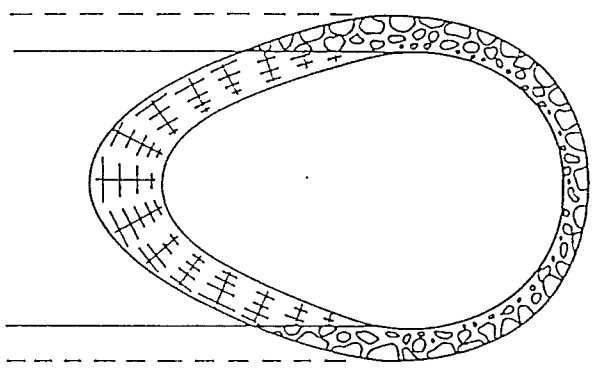

Figure 2.4 Schematic representation of the different weld pool zones. The narrow zone on the right represents the mushy zone [3].

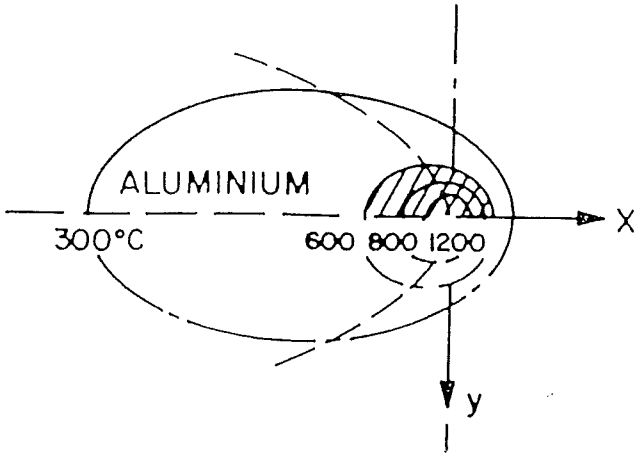

Figure 2.5 Temperature distribution in workpiece and weld pool (hatched) [5].

The heat input is defined by the following equation:

$$HI = \eta_p \frac{UI}{v} \quad (1)$$

in which HI is the heat input (J/mm), η_p is the process efficiency (fraction), U is the arc voltage (V), I is the welding current (A) and v is the travel speed (mm/s). The geometry and dimensions of the weld pool are mainly dependent on the heat input and therefore on the welding current, on the arc voltage and on the travel speed. Increasing the arc voltage or current, or decreasing the travel speed obviously results in an increase in weld pool size.

The weld pool geometry mainly varies with the travel speed: with increasing travel speed the electrode-weld system becomes more eccentric. The top view of the weld pool shape transforms from a circular shape at zero speed via an elliptic shape to a teardrop shape at high speeds (Figure 2.3 [3]). Furthermore, the thermal conduction of the base metal influences the geometry: a weld pool in a metal of very high thermal diffusivity (e.g. aluminium) retains an elliptic shape even at high travel speeds [4].

Another important aspect in the case of alloys is the existence of a freezing range. The freezing range has a considerable influence on the transition zone between the molten metal and the solid metal (fusion boundary). For pure metals, the fusion boundary is well-defined and rather sharp. In the case of alloys, however, there is a zone, referred to as the mushy zone, with partially molten alloy (Figure 2.4 [3]). The fluid fraction in this zone varies from 100% at the weld pool side to 0% at the base metal side. Obviously, its size increases with an increasing freezing range and a flatter temperature gradient. As the temperature in the weld pool is lowest in the mushy zone and solid particles are present, the viscosity there is highest.

The temperature distribution in the weld pool and in the workpiece can be seen in Figure 2.5 [5]. At the front of the weld pool the isothermal lines are very close together, indicating a steep temperature gradient. This gradient increases with increasing travel speed and plate thickness, and with decreasing thermal diffusivity. The temperature gradient at the back of the weld pool is flatter than at the front, due to the movement of the arc. Increasing the travel speed, therefore, results at the back of the pool in a further reduction of the temperature gradient. The influence at the back of the weld pool of the plate thickness and of the thermal diffusivity is comparable to that at the front of the weld pool.

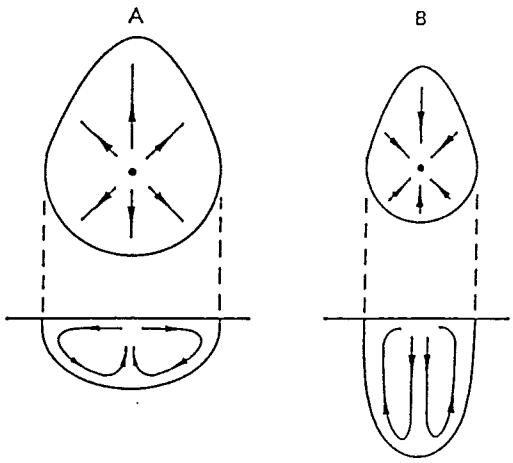

Figure 2.6 The two main flow types inside a weld pool (top and cross-section view) [3].

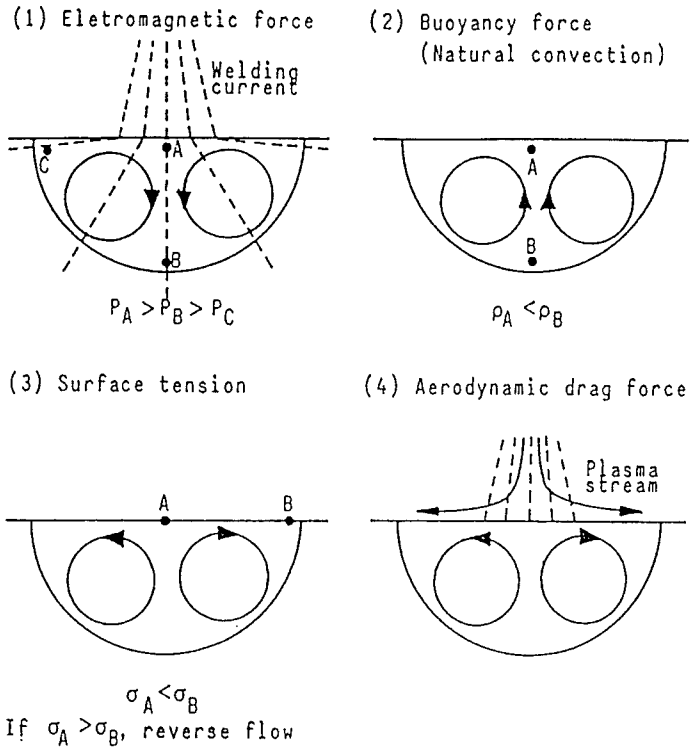

Figure 2.7 Four flow-inducing forces and the resultant flow type inside a weld pool [6].

Finally, the geometry and dimensions of the weld pool are determined by convective fluid flows occurring in the weld pool. Two main types of flow can be distinguished (Figure 2.6 [3]):

- type A: a radially outward- and in the centre of the weld pool upward directed flow resulting in a relatively wide and shallow weld pool,
- type B: a radially inward- and in the centre of the weld pool downward-directed flow, resulting in a deep and relatively narrow weld pool.

In a TIG weld pool without filler wire addition, fluid flow is mainly induced by four forces [3,6]. The flow type resulting from each separate force is depicted in Figure 2.7 [6].

Flow results from:

- electromagnetic forces, due to the diverging electrical current and the induced magnetic field in the weld pool. These forces generate a Lorentz flow of type B.
- buoyancy forces, due to variations in the density of the liquid metal, caused by the local variations in temperature. These result in natural convection of type A.
- gradients in surface tension along the surface of the weld pool. These gradients are induced by gradients in temperature (as the surface tension is temperature dependent) or by gradients in solute content (especially surface active elements (surfactants) such as sulphur and oxygen). For pure metals, the surface tension decreases with increasing temperature, causing a Marangoni flow of type A. However, in the case of alloys with added surfactants, the surface tension initially increases with temperature, but decreases again at higher temperatures. At lower temperatures, this results in a fluid flow of type B, at higher temperatures in a fluid flow of type A. It is also possible, that both types of flow are found to exist next to each other within one weld pool.
- aerodynamic drag forces, due to plasma jet and shielding gas flow along the weld pool surface. These forces generate a radially outward-directed fluid flow of type A.

The first two forces listed above are body forces, acting on the bulk of the weld pool; they have the greatest influence in TIG welding. Of these two, the Lorentz flow dominates at high welding currents, whereas the natural convection dominates at low welding currents. The second pair of forces are shear forces only acting on the weld pool surface.

According to Willgoss [7], a stable fluid motion is not to be expected during normal TIG welding, because a single structurally dominating force is absent. However, inside the weld pool, there will always be a net rearward fluid flow, as the pool moves over the workpiece and metal is melted at the front while solidification takes place at the back.

2.5. The solidification of weld metal

The actual joint is formed as the molten weld metal solidifies. The final structure of the weld metal appears to be determined by the weld pool geometry and the weld pool dimensions. This section discusses the elementary features of weld metal solidification. Firstly, it reviews the macrostructure of the weld metal. Secondly, it focuses on the microstructure. Finally, it briefly discusses several conditions favouring the formation of equiaxed grains, as these grains give a weld good properties.

- Macrostructure

In weldments, one may distinguish a primary, a secondary and a tertiary structure. The primary structure is the first structure created directly upon solidification. The secondary structure can be observed after a phase transformation has taken place, for instance the austenite-ferrite transformation in ferritic weld metal. The tertiary structure can be found in a multi-pass weld: due to a later weld pass, the previously deposited metal is heat treated. In this section, only the primary structure is discussed, as this is the only structure that can be influenced by EMS.

The three main stages of (primary) solidification are epitaxial growth, competitive growth, and nucleation of new grains [8]. In general, solidification involves the formation and growth of nuclei. During welding, by contrast, the formation of nuclei is of minor importance, as the solid-liquid interface acts as an ideal substrate.

Solidification starts with epitaxial growth: the existing crystalline substrate at the fusion boundary is extended with atoms from the melt, without a change in crystallographic orientation. Furthermore, the grain width of the new grains is copied from the grain width of the substrate.

The second stage of the solidification process is dominated by competitive growth. Competitive growth results from two phenomena. Firstly, crystals exhibit

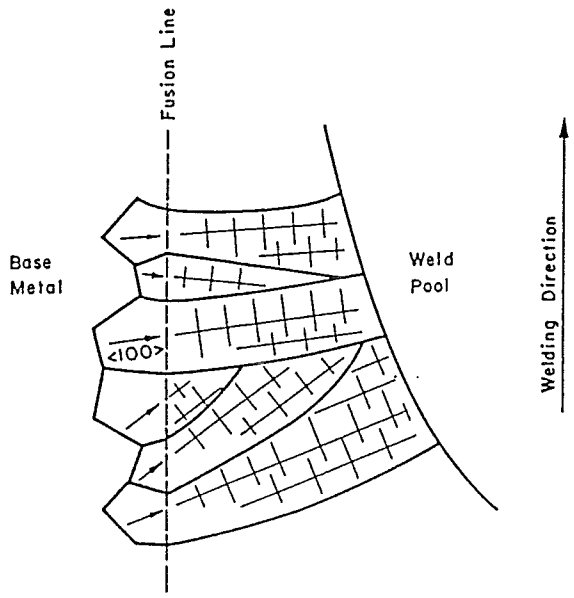

Figure 2.8 Epitaxial and competitive growth: favourably orientated grains crowd out others [8].

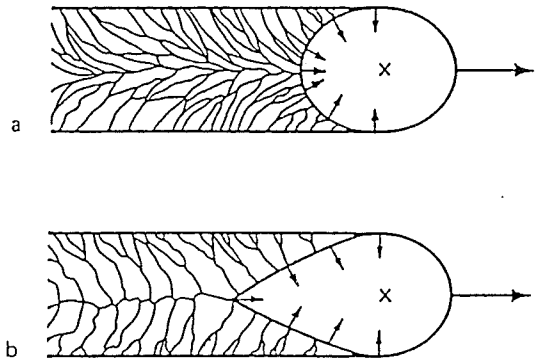

Figure 2.9 Macrostructure in the case of:
a: an elliptic-shaped weld pool,
b: a teardrop-shaped weld pool [3].

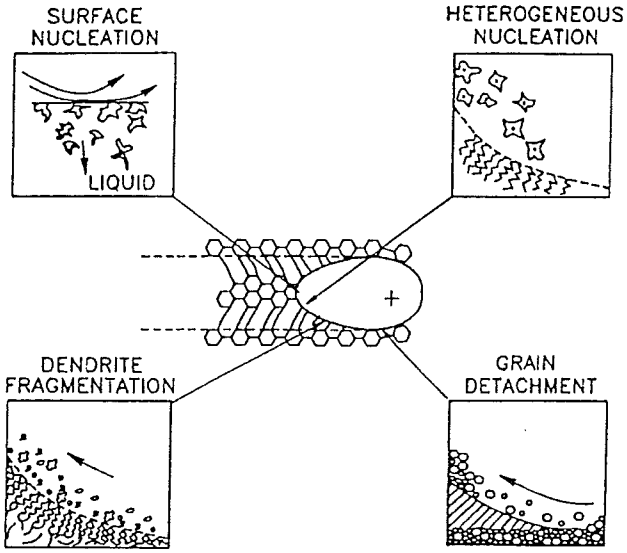

Figure 2.10 Four mechanisms providing nuclei in the weld pool [4].

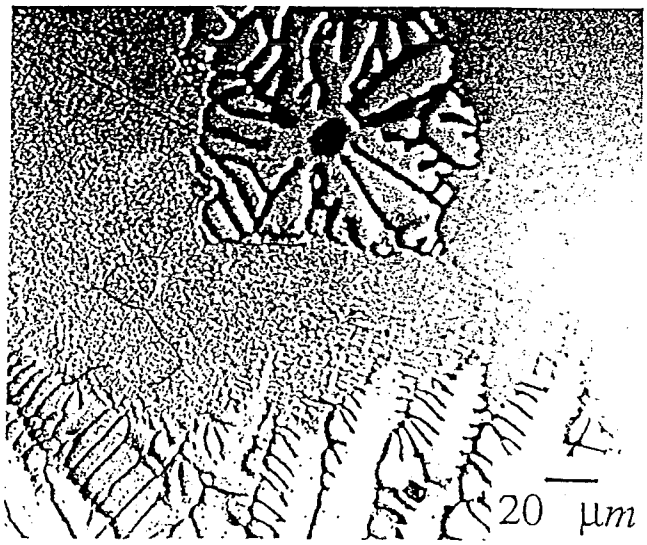

Figure 2.11 An example of an equiaxed dendrite in ferritic stainless steel [4].

crystallographic easy-growth directions (<100> for fcc and bcc crystals and <1010> for hcp crystals). Secondly, the grains grow preferably along the steepest temperature gradient, because in this direction heat removal is quickest. Therefore, grains with their crystallographic easy-growth direction more or less parallel to the steepest temperature gradient tend to grow easiest and they dominate and crowd out other grains (Figure 2.8 [8]).

As the steepest temperature gradient is perpendicular to the pool boundary, it is clear that the weld pool geometry influences the primary structure. In a teardrop-shaped weld pool, the columnar grains continue to grow from both sides of the weld, until they meet at the weld centreline. This is due to the fact that the thermal gradient remains fairly constant (i.e. perpendicular to the more or less angular backside of the teardrop-shaped pool) up to the weld centreline. If this is the case, the weld exhibits a completely columnar structure, with a distinct plane along the weld centreline, which is very susceptible to (solidification) cracking. In a more elliptic-shaped weld pool, however, the maximum temperature gradient changes direction going from the fusion boundary to the centre, as the pool backside has a constantly changing curvature. The inward growing grains follow this orientation, resulting in bent or even refined grains. Columnar grains resulting from an elliptic-shaped and from a teardrop-shaped weld pool can be seen in Figure 2.9 [3].

A totally columnar structure only occurs if nucleation in the bulk of the liquid - the third stage of primary solidification - does not take place. If it does take place, new grains may disturb the growth of columnar grains or even block them off.

This nucleation in the bulk is expected to result mainly from the following four mechanisms [4,8] (Figure 2.10 [4]):

- dendrite fragmentation,
- grain detachment,
- heterogeneous nucleation,
- surface nucleation.

As the first two mechanisms listed above are not very likely to occur in a normal TIG weld pool, due to its small size and its mild fluid flow, they are not further discussed in this section. They are discussed in Chapter 3, however, because they can be promoted by EMS.

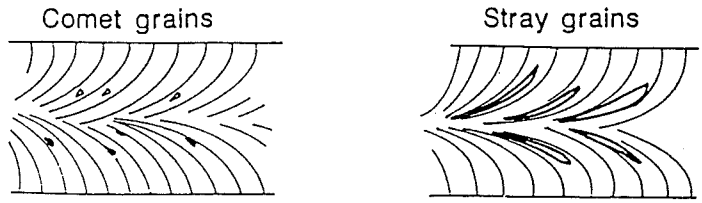

Figure 2.12 Schematic representation of comet grains and stray grains [9].

Figure 2.13 Feathery grain structure (centre) in a weld of AA2014 aluminium alloy [10].

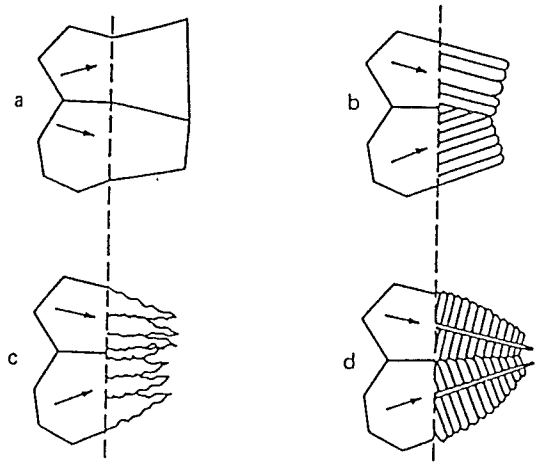

Figure 2.14 Different substructures of weld metal: a: planar, b: cellular, c: cellular-dendritic, d: dendritic [3].

The third mechanism, heterogeneous nucleation, can be characterised as nucleation on "foreign" particles, for instance non-melting impurities. It is promoted by (constitutional) supercooling, which is explained below. Apart from heterogeneous nucleation, homogeneous nucleation can take place. Homogeneous nucleation is defined as spontaneous nucleation in the liquid metal, simply due to supercooling (i.e. without the help of an existing solid particle). In welding, however, heterogeneous nucleation generally takes place before homogeneous nucleation can occur.

The last mechanism, surface nucleation, results from the high cooling rate at the weld pool surface, due to the cooling effect of the shielding gas. Thus solid nuclei can form, and shower down the weld pool, acting as nuclei for new grains [9].

The newly formed grains can be of various types: equiaxed, comet, stray or feathery. Randomly orientated equiaxed grains (Figure 2.11 [4]) normally only form near the weld centreline, due to the favourable local solidification conditions there present. Conditions favouring the formation of these grains are further discussed below, as small equiaxed grains give the weldment very good mechanical properties.

Comet grains are small grains which are not quite equiaxed, but have a tail pointing towards the heat source. If these grains grow over a considerable distance, they are called stray grains [9]. Both comet and stray grains can be seen in Figure 2.12 [9].

Finally, feathery grains (Figure 2.13 [10]) are formed through twin growth. They are large grains which have a feather-like form and are built up of small lamellae. These lamellae have a dendritic substructure, but the angle between the primary and the secondary dendrite arm is smaller than the usual straight angle [11]. A feathery grain structure results in inferior mechanical properties of the weld. Feathery grains are very common in some aluminium alloys (e.g. 5xxx-series).

- Microstructure

Within the primary structure, several substructures (microstructures) can be found: planar, or if the planar solidification front brakes up due to constitutional supercooling: cellular, cellular-dendritic and dendritic (Figure 2.14 [3]). Which microstructure is formed, depends on the alloying concentration and on the G/R ratio (Figure 2.15 [3]). Both constitutional supercooling and the G/R ratio are explained below.

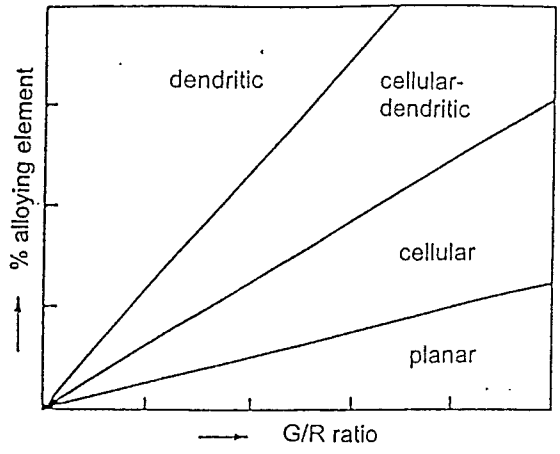

Figure 2.15 Schematic representation of the influence of the chemical composition and the G/R ratio on the microstructure of the weld metal [3].

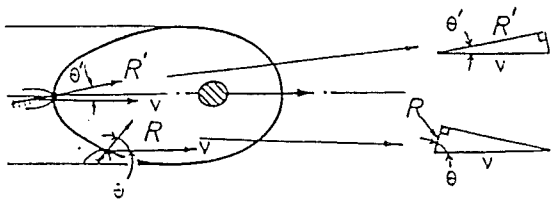

Figure 2.17 The solidification rate R as function of its position and of the travel speed v [5].

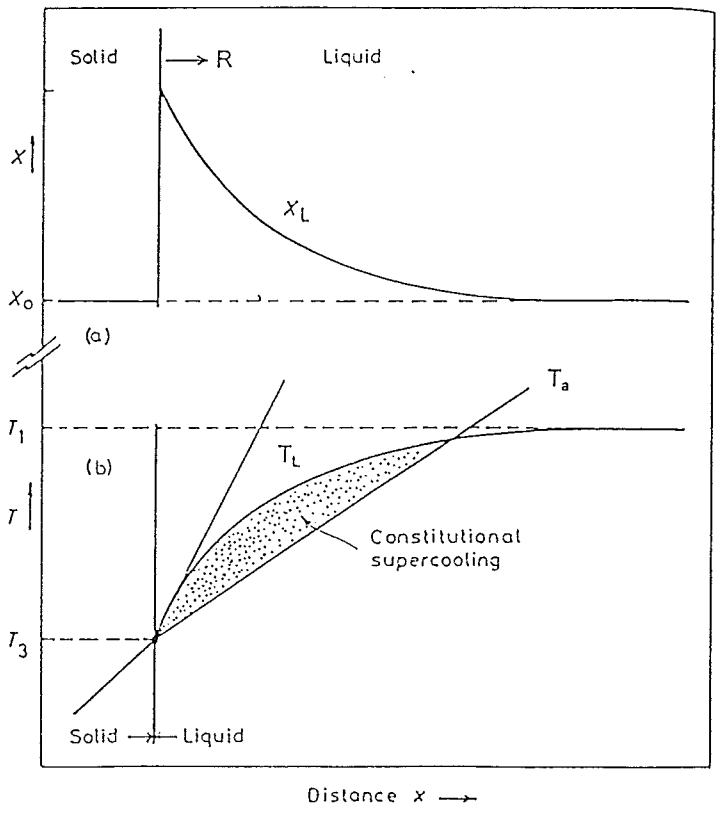

Figure 2.16 The origin of constitutional supercooling: a: the composition profile ahead of the solidification front, b: the actual temperature profile T_a and the liquidus temperature profile T_L [5].

Constitutional supercooling is explained with the help of Figure 2.16 [5] for a hypothetic binary alloy. During solidification, the (planar) solidification front moves with a certain speed R. Because the solvability of the alloying element is higher in the molten than in the solidified metal, the element diffuses out of the solid into the melt just ahead of the solidification front, resulting in a local increased concentration (X_L) of the alloying element. If no fluid flow occurs just ahead of the solidification front (which is very likely, due to the considerable viscosity), the resulting concentration gradient has to be resolved merely by diffusion. A steady state now occurs, when the increase in alloying element just ahead of the solidification front equals the decrease through diffusion.

The concentration increase results in a decrease of the liquidus temperature (T_L). Constitutional supercooling now exists when, as a result of the increase in the alloying element concentration, the metal has not yet solidified, although the actual temperature (T_a) is below the liquidus temperature. Constitutional supercooling is promoted by an increase in concentration gradient (therefore by an increase in the solidification rate R) and a decrease in the temperature gradient G (thus in a decrease in the G/R ratio).

Apart from aiding nucleation, constitutional supercooling can cause the planar solidification front to break-up, as mentioned above, resulting in the various substructures: cellular, cellular-dendritic or dendritic (Figure 2.14 [3]). It can be seen from this figure that the break-up of the planar front results in a finer microstructure, with the type of substruture mainly dependant on the chemical composition and the G/R ratio (Figure 2.15 [3]).

The solidification rate is commonly expressed as the G/R ratio, in which G represents the temperature gradient at the solidification front and R the velocity of the solidification front. R can be calculated from the travel speed with help of the following equation [3-5]:

$$R = v \cos\vartheta \qquad (2)$$

in which v is the travel speed (mm/s) and ϑ is the angle between the welding direction and the solidification direction (degree). (Figure 2.17 [5]).

Besides constitutional supercooling, segregation can be a result of the diffusion of alloying content into the liquid. Two types of segregation can be distinguished: micro-segregation and macro-segregation. Micro-segregation is characterised by changes in

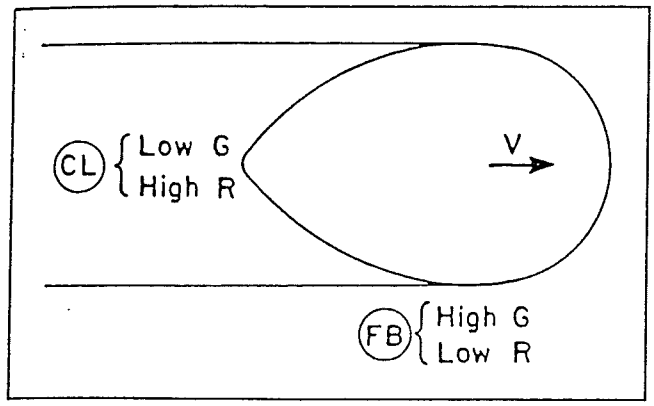

Figure 2.18 Schematic diagram showing the influence of the position on the G/R ratio (CL = centreline, FB = fusion boundary) [12].

chemical composition over very small distances of the order of the secondary dendrite arm spacing. Macro-segregation is characterised accordingly by composition changes over large distances of the order of the weld pool size.

Segregation, especially macro-segregation, is known to decrease both the mechanical properties and the corrosion resistance of the weld. For instance, in a totally columnar structure of a segregated alloy, the last amount of liquid metal to solidify at the weld centreline is very much enriched with alloying element, resulting in inferior properties.

- Influence of travel speed on the formation of equiaxed grains

Because equiaxed grains give the weld good properties, the influence of the travel speed on the fraction equiaxed grains is briefly discussed.

The process during which grain growth changes from columnar to equiaxed is called the Columnar to Equiaxed Transition (CET). Kerr [4,12] suggested two necessary conditions for CET to occur: the proper thermal conditions (i.e. a low G/R ratio) and a certain supply of nuclei. In a normal TIG weld, this transition can take place near the weld centreline, due to the change of the G/R ratio from the fusion boundary to the centreline (Figure 2.18 [12]). The G/R ratio decreases near the centreline due to two mechanisms. Firstly, the temperature gradient normal to the solid-liquid interface decreases from the fusion boundary towards the centreline. Secondly, the solidification velocity R increases, due to the diminishing value of ϑ (cf. Equation 1 and Figure 2.17 [5]) along the curved pool backside.

Close to the centreline, therefore, the lowest thermal gradient G and the highest solidification velocity R are present, favouring CET. As it is known that for the CET to occur nuclei are needed, an increase in the amount of (heterogeneous) nuclei also aids the formation of equiaxed grains.

Now let us return to the influence of the travel speed. Increasing the travel speed while maintaining a constant heat input to maintain the weld width, increases the equiaxed fraction, because it decreases G and increases R. The decrease of the thermal gradient G follows the increase in travel speed (cf. section 2.4), which also increases the solidification velocity R, as it is coupled to the travel speed through Equation 2. This results in a decrease in the G/R ratio, favouring CET.

However, if the travel speed is increased to a level where a teardrop-shaped weld pool is created, then ϑ has a considerable value (reducing R) and remains constant over much of the weld width. In that case, favourable conditions for CET do not occur.

It is believed that stirring of the liquid metal in the weld pool may change the thermal conditions in the weld pool, thus stimulating the formation of fine equiaxed grains. Furthermore, stirring is believed to be able to increase the supply of nuclei. This stirring can be induced by external magnetic fields. In the following chapter, therefore, the influence of external magnetic fields on the weld pool and on the welding arc are discussed, as are the resulting changes in the solidification structure and properties of the weld.

2.6. Hot cracking

In this project, one point of attention was solidification cracking, a type of hot cracking. This type of cracking is intergranular (i.e. along the grain boundaries), and most times along the weld centreline. Therefore it is also known as centreline cracking.

Solidification cracking takes place during the last stage of solidification, when a coherent interlocking network of primary dendrites is already formed separated by thin films of liquid [13]. Stresses are exerted onto this network due to further weld metal shrinkage, or due to the expansion of the base metal because of a continuing heat input (in case the welding continues), or due to a combination of both. When these stresses become too high, they cause the thin films to be ruptured. If sufficient liquid material is still available, the formed cracks can be filled up again ("healed"). However, if the stress relieve caused by these micro-cracks is not sufficient, a large, through-thickness crack will grow, combining separate micro-cracks.

A weld's propensity to solidification cracking depends on many factors. Most important is of course the chemical composition. For aluminium, there are two alloying boundaries to the area in which the weld is susceptible to solidification cracking [13]. The first one is obvious: if there are no alloying elements present, there will be no freezing range and hence no "thin film" along the grain boundaries. For the upper boundary, it can be said (very roughly) that there is no susceptibility, in case the alloying element concentration is high enough (let's say 6%) [13]. This can be seen in

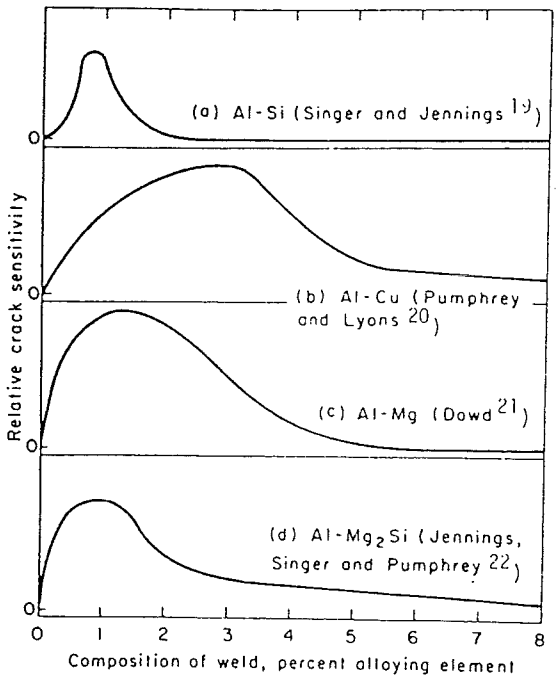

Figure 2.19 Relative solidification-cracking sensitivity as a function of alloying concentration [13].

Figure 2.19 [13] for some alloying elements. The reason for this is, that in these highly alloyed compositions, there is enough of the low melting liquid to heal the cracks. Other important factors are the weld geometry, the degree of restraint and of course the primary grain structure: small equiaxed grains make the weld less susceptible, because the network of primary dendrites is stronger, and there is a bigger area to harbour the low-melting phase.

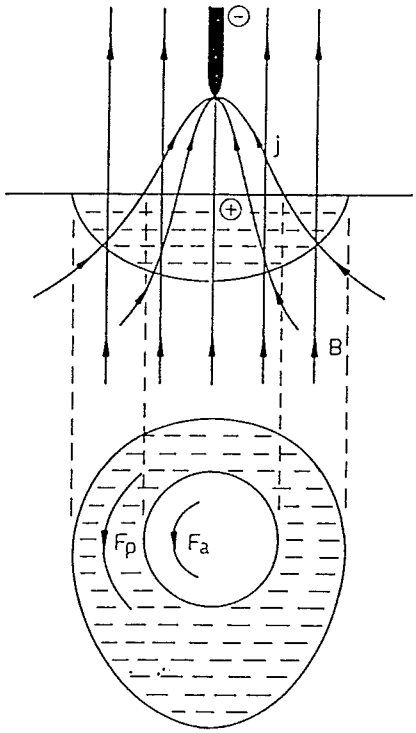

Figure 3.1 Schematic representation of the forces directing the molten metal and the welding arc in a rotational motion. j: current density, B: magnetic field induction, F_p and F_a: forces on the molten metal and on the arc, respectively. [15].

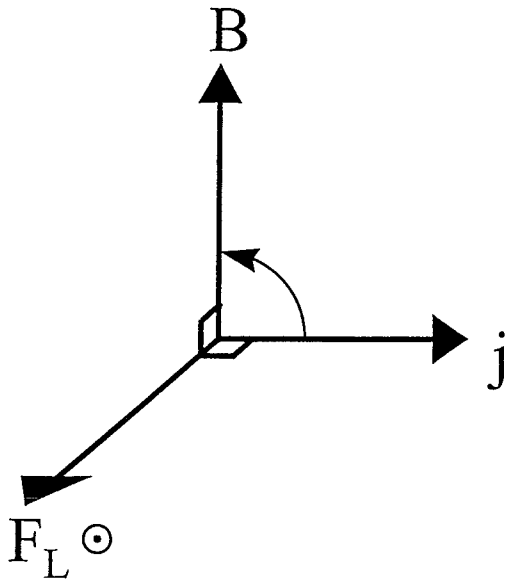

Figure 3.2 The relationship between the direction of the current density j, the magnetic induction B, and the Lorentz force F_L. If we rotate j over the smallest possible angle in the direction of B (clockwise or anti-clockwise), the Lorentz force operates perpendicular to both j and B, and in the direction a corkscrew goes, when rotated correspondingly.

3. The application of Electro-Magnetic Stirring during welding

3.1. Introduction

In this chapter, the application of Electro-Magnetic Stirring during arc welding is discussed. In the foregoing, the interaction between the electric current and the welding-current induced magnetic field was already mentioned. The resultant Lorentz force gradient in the welding arc (and the thus formed pressure gradient) results in a plasma jet. When external magnetic fields are applied, clearly comparable effects will occur. As both the welding arc and the weld pool are conducting an electric current, both are influenced by the magnetic field.

In Electro-Magnetic Stirring (EMS), the applied magnetic field is primarily used to directly influence weld pool flow. The use of EMS to improve weld properties was first suggested by Brown et al. in 1962 [14] after the electromagnetic stirring technique had already been in use for casting for several years.

3.2. Lorentz force

Weld pool flow is induced through Lorentz interaction between a magnetic field and the welding current (Figure 3.1 [15]). The direction of the field lines of the longitudinal (axial) magnetic field is (anti)parallel to the electrode axis. The Lorentz force (F_L) working on a volume dV of molten metal is a function of the magnetic induction (magnetic field strength, B) and of the current density (j), and it can be represented by the following vector equation:

$$\vec{F}_L = \vec{j} \times \vec{B} \tag{3}$$

The direction of the Lorentz force can be determined with help of Maxwell's rule (also known as Fleming's left hand rule and as the motor rule). This is illustrated in Figure 3.2. The magnitude of the Lorentz force is given by:

$$F_L = jB \cdot \sin\alpha \tag{4}$$

in which α is the smallest angle between the electric current density vector and the magnetic inductance vector. It is evident from this equation that the Lorentz force has

magnitude zero in those cases in which the electrical current and the magnetic induction are orientated (anti-)parallel (because then $\sin\alpha = 0$).

For the resultant fluid flow, two equations are of importance: the continuity-of-mass equation, which for a fluid of a constant density of mass (i.e. incompressible) simply is [16]:

$$\nabla \cdot \vec{v} = 0 \tag{5}$$

with v the velocity vector of the fluid.

The other equation of importance is the momentum equation, which for fluids of constant density of mass and viscosity is [2,16]:

$$\rho\left(\frac{\partial v}{\partial t} + v \cdot \nabla v\right) = -\nabla P + \eta \nabla^2 v + \rho\beta g_z (T - T_L) + \vec{j} x \vec{B} \tag{6}$$

with ∇P the static pressure force, $\eta\nabla^2 v$ the viscous force, $\rho\beta g_z(T-T_L)$ the buoyancy force and $\vec{j} x \vec{B}$ the Lorentz force. This equation, known as the Navier-Stokes equation, is therefore similar to Newton's equation relating acceleration and mass to (a sum of) force(s).

In case of a weld pool, the Navier-Stokes equation can best be written in cylindrical co-ordinates. The only term which then still keeps the Lorentz term, is the one for the azimuthal (θ) component. This is a consequence of the fact that the current density only has components in the axial (z) and radial (r) direction, whilst the magnetic induction (B) is purely axial (cf. Equation 3, 4 and Maxwell's rule). The azimuthal component of the Navier-Stokes equation then becomes [2,16]:

$$\rho\left(\frac{\partial v_\theta}{\partial t} + v_r \frac{\partial v_\theta}{\partial r} + \frac{v_\theta}{r}\frac{\partial v_\theta}{\partial \theta} + \frac{v_r v_\theta}{r} + v_z \frac{\partial v_\theta}{\partial z}\right) = -\frac{1}{r}\frac{\partial P}{\partial \theta} + \eta \nabla^2 v|_\theta + \vec{j}_r x \vec{B}_z \tag{7}$$

With EMS, the Lorentz force is in general greater than the other forces acting inside the weld pool. From Equation 7 it can then be seen that this results in a rotational motion of the molten metal, because the Lorentz force works in the azimuthal direction only. However, due to the travelling of the weld pool over the workpiece (resulting in a net rearward motion of molten metal within the weld pool), the weld pool flow is no longer purely rotational.

EMS can be performed as unidirectional or alternating stirring. In case of unidirectional stirring, the welding current and magnetic field are typically non-alternating, resulting in a constant rotation of the molten metal. In case of alternating stirring, typically either of

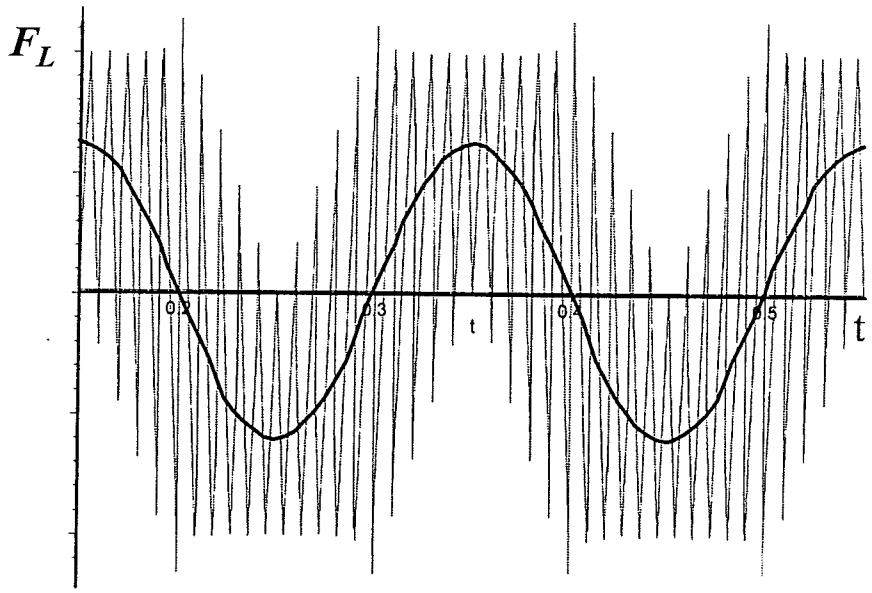

Figure 3.3 Graph of the Lorentz force versus time. The thick line represents the effective Lorentz force (i.e. the low-frequency component).

the two alternates at a low frequency. However, in the case of welding aluminium with alternating current, the frequency is too high (50Hz) to result in alternating weld pool flow, due to the fluids inertia. This problem can be solved by having the magnetic field alternate at a frequency only a couple of Hertz different from that of the current. This results in an alternating Lorentz force of an even higher frequency, but with a low-frequency component, which becomes clear when we write the wave-forms as Fourier series.

The current density has a square wave-form, provided by the power source used. This wave form can be written as a Fourier series [17]:

$$j(t) = j_0 \frac{4}{\pi} \sum_{n=1} \frac{1}{(2n-1)} \sin[2\pi(2n-1)\nu_j \cdot t + \varphi_j] \tag{8}$$

whereas the alternating magnetic field, which has a triangular wave-form, can be written as the following Fourier series [17]

$$B(t) = B \frac{8}{\pi^2} \sum_{m=1} \frac{1}{(2m-1)^2} \cos[2\pi(2m-1)\nu_B \cdot t + \varphi_B] \tag{9}$$

With help of Equation 4 and the following goniometrical equation:

$$\sin(x) \cdot \cos(y) = \frac{1}{2}\sin(x+y) + \frac{1}{2}\sin(x-y) \tag{10}$$

we can then write for the Lorentz force:

$$\begin{aligned} F_L(t) = j_0 B \sin(\alpha) \frac{32}{\pi^3} \sum_{n=1} \sum_{m=1} \frac{1}{(2n-1)} \frac{1}{(2m-1)^2} \cdot \\ \left\{ \frac{1}{2} \sin\left[2\pi[(2n-1)\nu_j + (2m-1)\nu_B]t + (\varphi_j + \varphi_B)\right] + \right. \\ \left. \frac{1}{2} \sin\left[2\pi[(2n-1)\nu_j - (2m-1)\nu_B]t + (\varphi_j - \varphi_B)\right] \right\} \end{aligned} \tag{11}$$

It can be seen from this equation, that the wave-form for the Lorentz force can be composed of sinusoidal waves, some with a high frequency, and some with a low frequency. The most important of both are those for which the summation indices m and n equal 1. The high-frequency component then has a frequency of ($\nu_j + \nu_B$), and the low-frequency component of ($\nu_j - \nu_B$) (Figure 3.3). Therefore, if the magnetic field alternates at a frequency just a couple of Hertz above that of the welding current, the low-frequency Lorentz force component will induce weld pool flow with an effective stirring

frequency ν_S which is (ν_j - ν_B), (or (ν_B - ν_j), as sin(-x) = -sin(x), and the Lorentz force is periodical). The high-frequency component will have a frequency, which is too high for the molten metal to follow, due to its inertia. This allows us to stir at a chosen, low frequency whilst still welding with an alternating welding current. According to De Vries [2], it is best to choose the frequency of the magnetic field higher than that of the welding current, to prevent interference of the high-frequency components of the magnetic field with the welding current.

This also means, that if both the magnetic field and the welding current have the same frequency, the low-frequency component of the Lorentz force has frequency zero, resulting in unidirectional stirring (but with the magnitude and direction of the Lorentz force dependant on the phase difference φ_j - φ_B).

In the next section, the influence of external longitudinal electromagnetic fields (as in EMS) on the weld pool behaviour and on the welding arc is discussed. Special attention is given to the fluid flow and the temperature distribution in the weld pool, and to the consequences for weld pool solidification.

3.3. Influences of Electro-Magnetic Stirring on the weld pool behaviour and on the welding arc

3.3.1. Influences of unidirectional EMS on the weld pool behaviour

These have already been extensively reviewed in my literature review on EMS and Magnetic Arc Oscillation [1]. Because this project focused on alternating EMS (with both alternating welding current and alternating magnetic fields), only the influence of alternating stirring is discussed here.

3.3.2. Influences of alternating EMS on the weld pool behaviour

To generate alternating stirring action, the input of the electromagnetic coils is an alternating current. Commonly, a square wave input to the coils is used, because this

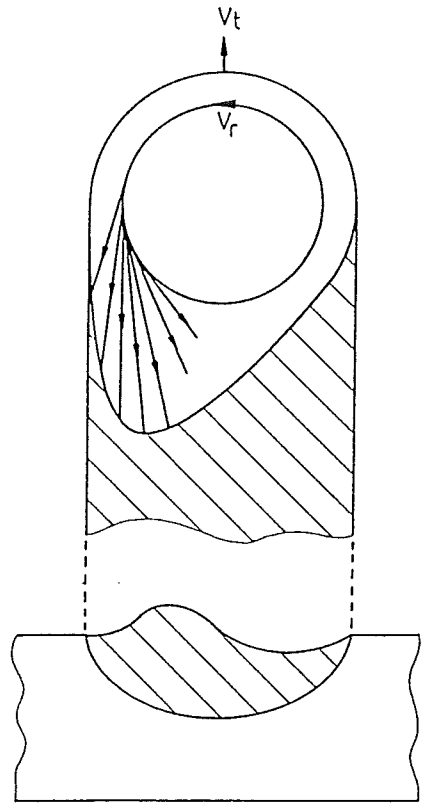

Figure 3.4 Schematic representation of the asymmetric weld pool shape (top view) and the ditch-dike effect (transverse cross-section. v_t: travel speed, v_r: rotational flow velocity of the liquid weld metal [15].

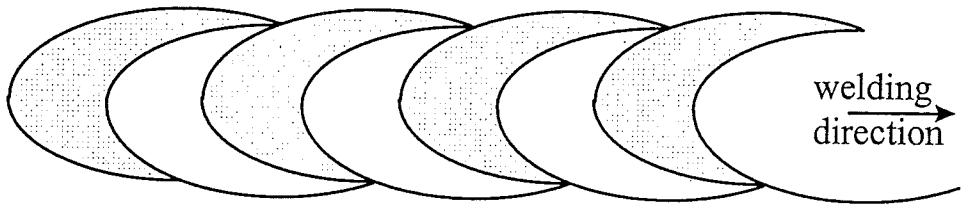

Figure 3.5 Schematic drawing of weld ripples and weaved fusion boundarie due to alternating stirring (top view).

input maximises the Lorentz force exerted on the molten metal in each periodic half cycle [12]. This project focuses on EMS with both the welding current and the magnetic field alternating, with the frequencies chosen in such a way, that the stirring action is comparable to low-frequency EMS.

- Weld pool flow

Due to the flow of hot liquid along either fusion boundary, the weld pool shape becomes asymmetric. The hot liquid melts its way along the fusion boundary and extends the weld pool on that side. This effect is increased by the fact that on the hot side, the rotational flow and the net rearward flow due to the travelling of the weld pool amplify each other, whilst on the colder side, both flows counteract each other. A schematic representation can be seen in Figure 3.4 [15], in which also the resultant ditch-dike effect is shown. The fluid flow velocity is in general thought to be considerable. Malinowksi-Brodnicka et al. [15] for instance expect it to be some 500 mm/s.

The periodic reversal in the direction of the Lorentz force results in the flow direction being periodically reversed as well. At relatively low frequencies, the fluid reversal has the same frequency as the Lorentz force. However, at high frequencies the fluid has difficulties following this frequency, due to its inertia.

The periodic change in fluid flow eliminates some of the generally unwanted effects that arise when a constant magnetic field is used: most importantly the ditch-dike effect changes side, gradually disappearing with increasing frequency.

The reversal of the flow direction in the weld pool can be seen on the weld surface as ripples and weaved fusion boundaries (Figure 3.5). Both effects diminish with increasing frequency. The weld centreline is also weaved, which can be advantageous in the case of a metal susceptible to solidification (or centreline) cracking as this type of crack grows intergranularly along the weld centreline (cf. Section 2.6.). Because of the weaved centreline, the total crack length is longer, and the crack constantly has to change direction, thus dissipating energy, which could reduce the crack length.

- Temperature distribution

Watanabe et al. [18] measured a transverse temperature distribution during welding of austenitic stainless steel by means of an infrared pyrometer. They found a considerable

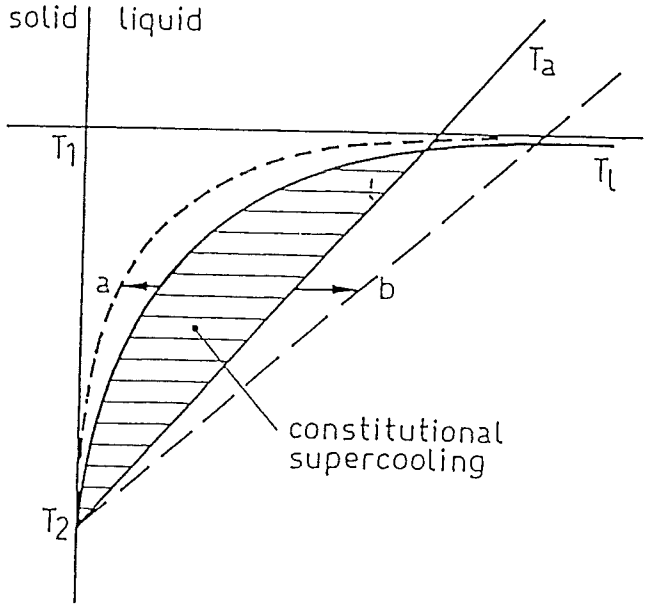

Figure 3.6 The influence of mixing of the liquid weld metal (a) and of temperature homogenisation (b) on constitutional supercooling ahead of the solidification front. (T_a and T_l are the actual temperature and the liquidus temperature, respectively) [15].

drop in temperature ahead of the solidification front, which reduces the temperature gradient at the pool boundary. (This, however, also means an increase in viscosity, making the stirring more difficult.)

Malinowski-Brodnicka et al. [15] stated, that EMS decreases the temperature gradient and makes the concentration gradient steeper, both ahead of the solidification front. From Figure 3.6 [15] this can be seen to increase the area of constitutional supercooling.

- Solidification

As mentioned in the previous chapter, there are two necessary conditions for the transition from a columnar to an equiaxed structure (CET) to occur: the proper thermal conditions (i.e. small G/R-ratio) and a certain supply of nuclei. An increase in constitutional supercooling, aforementioned to result from EMS, favours CET. EMS is furthermore believed to promote the second condition through the formation of nuclei. Two mechanisms are thought responsible, namely those mentioned in Chapter 2 as being not very likely to occur in a normal TIG weld pool: dendrite fragmentation and grain detachment. However, there is still some controversy whether these mechanisms (mainly dendrite fragmentation) actually take place during EMS.

Dendrite fragmentation is thought to result from the fluid flow, which is expected to be turbulent [2,12,19] under quite common EMS conditions. Some investigators expect the turbulent fluid motion able to mechanically break-off dendrite tips [8]. These tips are then transported to another section of the weld pool, where they can act as nuclei for new grains, but only if they do not totally remelt in hotter parts of the weld pool. However, another point of view is that the forces exerted onto the dendrites via the stirring are not high enough to mechanically break off dendrite tips [20]. Dendrite fragmentation could then occur via the melting off of secondary dendrite arms [8,20-22]. Dendrite arms can be molten off, because the root of a dendrite arm is in general thinner than the stem. Therefore, the tip will not have totally molten, when the root already has. This way of dendrite fragmentation is likely to happen with an alternating field, because then parts of the weld pool are alternatingly cooled and heated. The second mechanism, grain detachment, is the sweeping into the melt of partially molten grains from the mushy zone. These grains can then act as nuclei in other parts of the weld pool, also if they do not totally remelt [23]. According to Pearce and Kerr [23], this mechanism only operates well, if grain growth in the heat affected zone is restricted,

because otherwise the grains are too big to be detached by the fluid motion. It is also more likely in alloys with a large freezing range, because these have a larger mushy zone. The large freezing range probably results in a low viscosity of the molten metal in-between the grains as well.

However, these mechanisms providing nuclei and thereby refining the grain size are quite debatable. It should be kept in mind that other mechanisms may play a vital role. Especially the existence of heterogeneous nuclei can obscure the nuclei providing effect of EMS, that is whether or not grain detachment and dendrite fragmentation actually take place. For instance, the presence of solid titanium particles in the weld pool is expected to be the main nucleation mechanism in the grain refinement of steels and of aluminium alloys [23]. Nevertheless, this nucleation can be aided by the changing thermal conditions in the weld pool, resulting from EMS.

Another way in which EMS can cause grain refinement is solely by changes in the temperature gradients resulting from alternating stirring. The hottest fluid in the weld pool (from the front) is alternatingly transported along either fusion boundary. This results in directional changes in the steepest temperature gradient, ahead of the solidification front. As it is known that grains preferably grow along this steepest temperature gradient, this hinders growth of grains over longer distances. When the temperature gradient changes direction, the initially favourably orientated grains are hindered in their growth, facilitating new grains to take over. (This effect is comparable to the grain refining effect resulting from an elliptic-shaped weld pool rather than a teardrop-shaped one, as mentioned in section 2.5.) For this kind of grain refinement, Matsuda [21] defined the optimal frequency as that frequency for which the length of the ripples equals the width of the grains, as this would render "equiaxed" grains.

3.3.3. Influences of alternating EMS on the welding arc

The welding arc conducts the electric current between the cathode and the anode. Therefore, although the primary target of EMS is to influence weld pool behaviour, the arc is influenced as well in a manner, comparable to that of the weld pool.

If the arc is symmetric with respect to its axis, it just starts to rotate in an axial magnetic field, similar to the liquid metal in a stationary, circular weld pool. Clearly, the

speed of the rotation increases with increasing magnetic field strength and welding current. Due to the centrifugal forces, the arc broadens and becomes conical in shape and the luminosity of the outer part of the arc becomes much higher than that of the arc centre; a sort of hollow arc is formed [15]. This was found for submerged arc welding too, by Jia and Xiao [24].

If the arc is not symmetric with respect to the electrode axis, the arc does not only rotate, but the anode spot will move over the workpiece as well. This will cause arc instabilities and can even cause arc blow.

The arc motion has an additional effect on the weld pool motion. Arc rotation increases the corresponding movement of the molten metal in the weld pool due to the drag force. If the anode spot moves over the object, this also influences the weld pool behaviour, though in a somewhat less predictable manner. The changed heat input, however, which results from the movement of the anode spot, can have a significant influence on solidification.

Table 1: Chemical composition of Alusuisse AA6082 T6 alloy as determined with XRF.

element	Mg	Si	Mn	Fe	Cu	Ti	Cr	Zn	Ni	Sn	Pb
weight %	0.92	0.86	0.65	0.38	0.05	0.02	0.01	0.01	<0.01	<0.01	<0.01

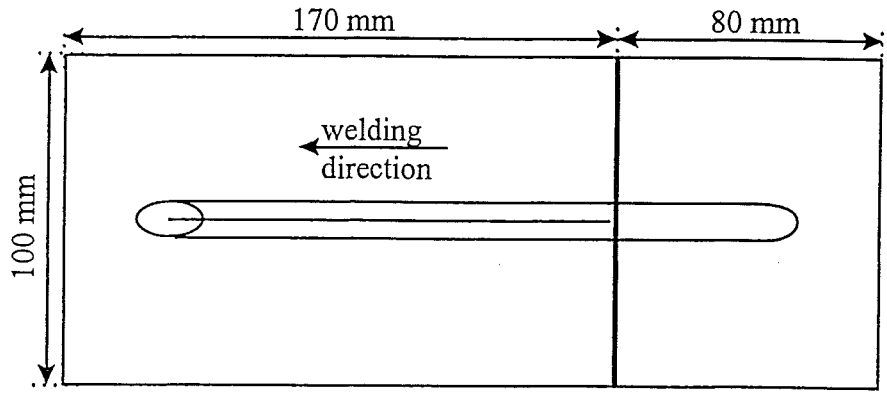

Figure 4.1 Geometry of plates used for solidification cracking investigation.

4. Experimental set-up and calibration

4.1. Introduction

This chapter covers the experimental set-up of the project. Firstly, in Section 4.2, the welding material is described, giving special attention to the geometry of the sample plates. Section 4.3 is on the general welding set-up. In the next section, the generation of the magnetic fields is discussed as well as the calibration of the coils. The last section describes the sample preparation for optical analysis.

4.2. Specimen geometry

Bead-on-plate welds were made parallel to the rolling direction on AA6082 T6 aluminium plate. The chemical composition of the plate is listed in Table 1. The dimensions of the plates were 100x250 mm, with a thickness of 3 mm. Plates for the investigation of the solidification crack susceptibility consisted of two pieces, a starter plate of 100x80 mm and a welding plate of 100x170 mm, as the plate was cut perpendicular to the welding direction (Figure 4.1). This configuration has multiple advantages. Firstly, it diminishes the influence of the waiting time after the arc has been ignited. The workpiece is then kept stationary underneath the torch. This waiting time is needed to form a proper weld pool and to get full weld penetration. However, it also has considerable influence on the weld properties, because during this time the plate is preheated, which for instance is known to decrease the hot cracking susceptibility. Furthermore, the amount of preheat during this waiting time is very irreproducible. However, if arc ignition and waiting are performed on the starter plate (100x80 mm), the heat does hardly flow into the welding plate, on which the weld that will be examined is made.

Secondly, the ignition with the carbon stick contaminates the weld pool and sometimes influences its shape considerably. By starting the welding on the small starter plate, the weld pool will have a proper shape and will have been cleaned by the time it reaches the welding plate.

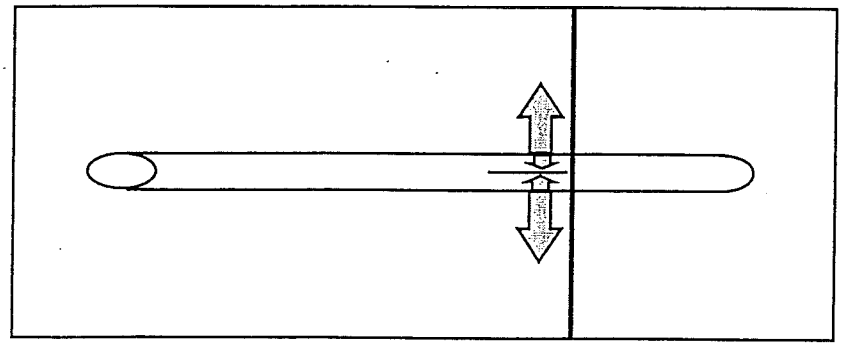

Figure 4.2 Schematic drawing indicating the expansion directions causing solidification cracking.

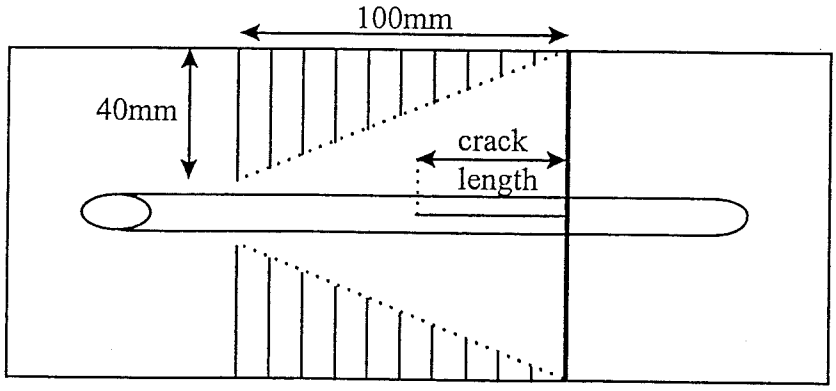

Figure 4.3 Geometry of Houldcroft specimen.

Lastly, the cut perpendicular to the welding direction acts as an initiator for the hot crack to grow from, because of two main reasons. Firstly, it provides a sharp point at which a stress concentration can build up, facilitating crack initiation. Secondly, because of the "U-shape", the thermal stress due to expansion of the base metal has to be borne by the weld alone (Figure 4.2).

To study the influence of EMS on the grain structure of the weld, welds were made on uncut plates. Similar settings were used as for the welds on the two-pieced plates. This way, no crack grows, which allows easier investigation of the microstructure.

The sample was placed on a (ferromagnetic) steel underplate with a milled groove to allow weld sagging and it is bolted down with six clamps (bolts and clamps made of austenitic stainless steel to not interfere with the magnetic field). The reason for bolting down the plate is that thus stress relieve through buckling of the plate is prevented, which would make hot cracking less likely to occur. Furthermore, it ensures close contact between the two plates in the case of the starter and welding plate, improving the continuity of the welding process. However, the plate could still expand, which is necessary for the hot cracking to occur.

For more quantitative measurements of the hot-cracking susceptibility, Houldcroft (fish-bone) specimens were used (Figure 4.3) [25]. These specimens have from the two sides slots of increasing length perpendicular to the welding direction. Thereby, the effective plate width is reduced along the weld, diminishing the stress resulting from the thermal expansion. (Slots are used in stead of a tapered plate, because the slots ensure that the heat-absorbing capacity of the plate is similar to that of a normal plate, allowing for a constant weld penetration.) Due to the stress relieve along the weld, the hot crack should stop at some point. The resultant length of the hot crack is a quantitatively comparable measure for the hot cracking susceptibility.

4.3. Welding

TIG-welding was performed with a pure tungsten electrode of 4 mm in diameter with a rounded tip. The set-up is shown in Figure 4.4. The electrode sticks 3 mm out of the gas cup, which has an internal diameter of 11 mm. During welding, argon was used as shielding gas at a flow rate of 10 l/min. The distance between the tip of the electrode

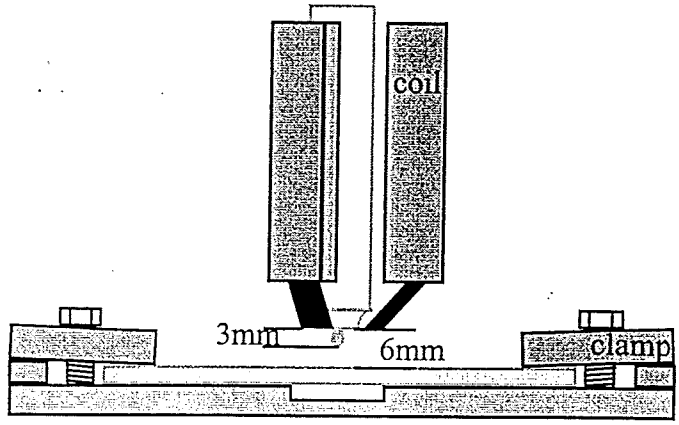

Figure 4.4 Schematic drawing of the experimental set-up (side view).

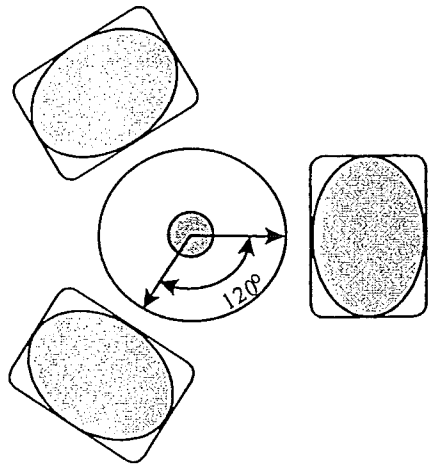

Figure 4.5 Schematic drawing of the welding torch and electromagnetic coils (top view).

and the specimen was 3 mm. The sample was placed on a traverse, with the electric ground located at the front. Alternating current was used to break down the oxide layer on the aluminium weld pool. The welding current was provided by an ESAB DTA 300 current source. The arc was ignited manually with the use of a carbon stick, after which the plate was kept stationary for a couple of seconds to allow a proper weld pool to be formed. Then the sample plate was moved on the traverse underneath the torch. During welding, the welding current and arc voltage were monitored. In between two welds, the steel underplate was cooled down to room temperature in water.

Welds have been made at different travel speeds: 4, 6, 8 and 10 mm/s. The current was chosen in such a way, that complete weld penetration was just reached for all travel speeds. For the different experiments at a set travel speed, the welding current was not altered. Evidently, the welding current used increased with travel speed (linearly as a matter of fact). For examination of the grain structure, welds have been made at 4 and 8 mm/s on uncut plates, therefore without hot cracks.

4.4. Magnetic fields

For the generation of the axial magnetic field, three coils were used, placed at regular intervals (120°) around the torch (Figure 4.5). The coils were connected in series and were fed with a current, generated on the computer as a square wave by a LabVIEW card and amplified by an audio amplifier. At the frequencies used (50-60 Hz, frequency of the magnetic field higher than that of the welding current, to not have the high-frequency components of the magnetic field interfere with the current), due to the build-up of the magnetic field and self-inductance of the coil-ferromagnetic coil system [2], this results in a triangular wave for the magnetic field. The LabVIEW programme controlling the magnetic field/coils was written in such a way, that it first checks whether a stable arc is ignited. This is performed by verifying that the measured arc voltage is within set boundaries. Then, after a set waiting period (mostly a waiting period of zero seconds was used) a square wave input to the coils is generated with the desired frequency but with a small amplitude. During a set time, the amplitude of the wave is slowly increased to the desired value, so as not to disturb the arc to much or even extinguish it through magnetic arc blow.

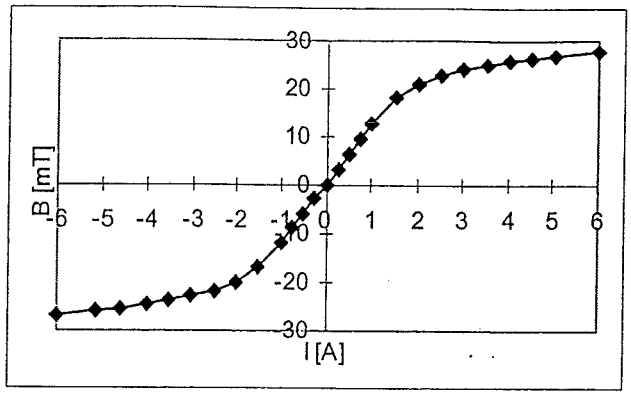

Figure 4.6 Saturation for three coils.

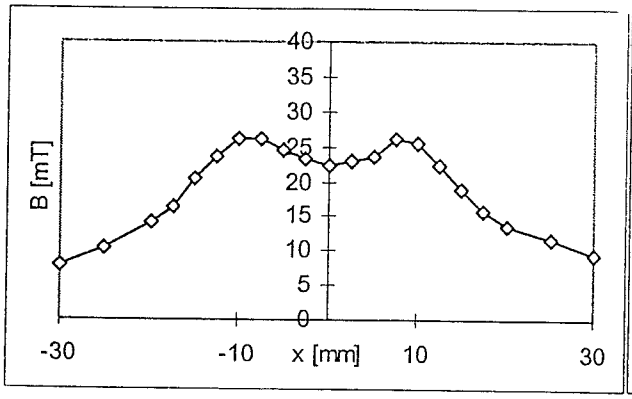

Figure 4.7 Magnetic field strength versus distance from the electrode (parallel) at 50 Hz.

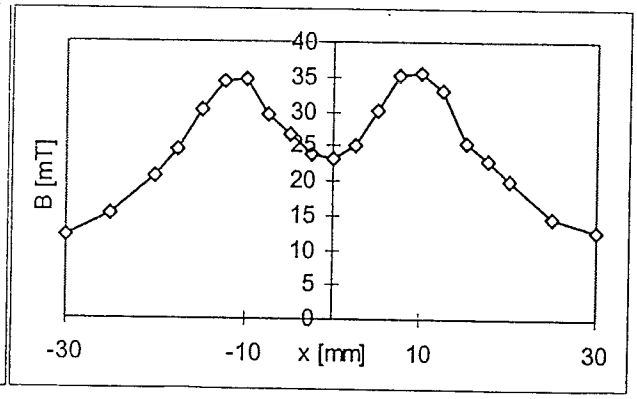

Figure 4.8 Magnetic field strength versus distance from the electrode (perpendicular) at 50 Hz.

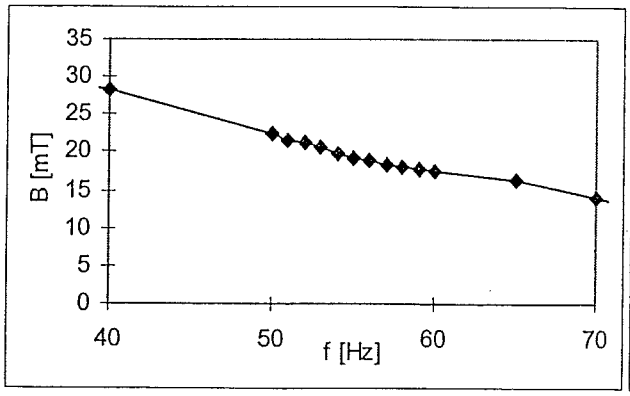

Figure 4.9 Magnetic field strength under the electrode versus frequency.

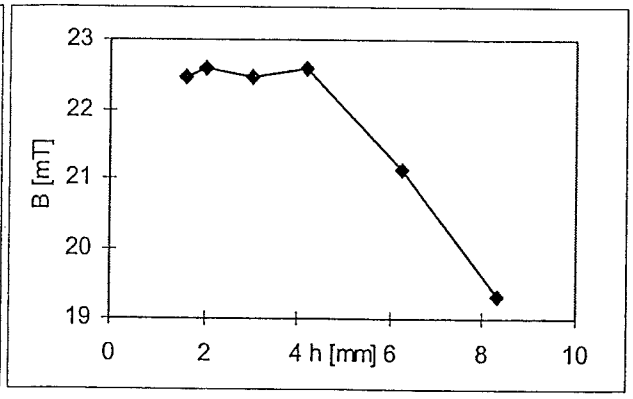

Figure 4.10 Magnetic field strength under the electrode versus arc length at 50 Hz.

The coils have ferromagnetic cores, which stick out of the coils and end next to the gas cup to concentrate the field around the weld pool. For the same reason a ferromagnetic underplate was used, drawing the field down, thus preventing the fanning-out of the field to the sides, which would diminish the effective magnetic field strength. The coils were cooled with compressed air.

The magnetic field was calibrated with a Lohet II linear Hall-probe. Firstly, the saturation value for the three magnetic coils was determined directly under the electrode on a sample plate. The distance between the sample and the electrode was set at 3 mm and the Hall-probe was placed in-between, directly on the sample. Then a direct current was applied to the coils, and the resultant magnetic field strength was measured. The results can be seen in Figure 4.6. It can be seen that saturation was reached at about 30 mT.

Secondly, the strength of the magnetic field was measured as a function of the distance from the electrode. This was performed in two directions: parallel and perpendicular to the welding direction (again with an "arc length" of 3 mm). The frequency for the generated square wave was 50 Hz, the amplitude was set to 5 V and the amplification factor was 15. The results of these measurements are presented in Figure 4.7 and Figure 4.8. It can be seen in these figures, that perpendicular to the welding direction higher peaks are reached next to the electrode. This is due to the milled groove in the underplate: the magnetic field is drawn to the underplate, especially to the sides of the groove, where the ferromagnetic material is in direct contact with the aluminium plate, and closest to the coils. Furthermore, the maximum value for the magnetic field directly under the electrode is lower than that measured in the previous measurement, because alternating current is fed to the coils. The influence of the frequency on the maximum field strength under the electrode is visualised in Figure 4.9 (again for an arc length of 3 mm, an amplitude of 5 V and an amplification factor of 15).

Lastly, the influence of the distance between the sample and the electrode (and therefore the coils and poles) was measured, at similar settings as before. Figure 4.10 shows that the strength of the magnetic field decreases with increasing distance. However, at low arc lengths, there is hardly any influence.

For the stirred welds, the one parameter of importance was the stirring frequency. This was generally between 0.5 and 10 Hz. For most of the welds, the magnetic field was activated when the weld was still entirely on the small starter plate.

The magnetic field strength was not altered for the different travel speeds. As a result, the magnitude of the Lorentz force (=j•B) was also different at different travel speeds. However, trying to use the same magnitude of the Lorentz force for different travel speeds could only have been realised by diminishing its value at higher travel speeds. This would also have increased the time during which no stirring occurs due to the reversal of the Lorentz force and the fluids inertia, while this becomes of course of increasing importance at higher travel speeds. Similarly, the magnetic field strength was not altered to compensate for the effect of the frequency has on it, as this could only have been performed by reducing the magnetic field strength even further at low frequencies.

4.5. Optical analysis

To study the influence of EMS on the structure of the weld metal, specimens of the welds have been examined (cross-sections and sections parallel to the weld surface). The specimens were ground (down to Grit 600), polished (down to 1μm) and etched. To reveal the grain structure, the samples were etched anodic using Barker's etch [26].

The anodic etching method of Barker is based on the fact that although aluminium is optically isotropic, aluminium oxide is not: it has the nature of double refraction. This means that a plane polarised beam striking an aluminium oxide film is rotated and undergoes some phase retardation before it is being reflected. This rotation and phase retardation of the incident beam results in an angular shift and broadening of the reflected beam. After passing through a cross-polariser, the light intensity is dependant on the amount of rotation and retardation. This in its turn is dependant on the orientation of the crystal face it strikes upon. Furthermore, the crystal face orientation of the aluminium oxide film is directly related to the original orientation of the underlying aluminium crystal face. Therefore, the differently orientated grains of the specimen can be made visible by covering them with a thin oxide film.

Such a thin oxide film was produced anodic: the specimen was used as the anode in an electrolytic cell. For a cathode, a strip of aluminium of the same alloy was used. The electrolyte was a solution of 2 % fluoboric acid (HBF_4) in distilled water. Fluoboric acid combines the gentle etching action of hydrofluoric acid and the oxide-film producing action of boric acid. The thickness of the oxide film is directly related to the

current density and to the etching time. Therefore, while the etching voltage was circa 30 V, the current depended on the specimen size. An oxide film of the correct thickness can be seen as an bluish glow on the specimen, whereas excessive etching produces a white layer. Because the thickness of the film can be increased by etching for a second time, it is best to start with a short etching time only. If further etching then proves necessary, the specimen can be etched again. While etching, stirring is not necessary, because the gas formation at the surfaces is quite turbulent. After etching, the specimens were cleaned ultrasonically in alcohol to remove all electrolyte (particularly from pores and cracks) and it was then blown dry, after which it is ready for microscopic examination.

Because the specimens were etched anodic, a small metal thread had to be spot-welded to the back of it, to conduct the electric current. It was then embedded in Technovit 4071 (an open-air, cold-curing resin) with the isolated thread sticking out of the back.

The optical analysis has been performed on a Jena Neophot 30. The pictures have been taken using Polaroid Black and White Instants.

5. Results and discussion

5.1. Introduction

In this chapter, experimental results are presented and discussed. For close observation of the effects of EMS, welds at travels speeds of 4 and 8 mm/s have been studied. The welding current for both travel speeds was chosen in such a way that weld penetration was similar. With regard to the hot-cracking susceptibility, the effects of EMS have also been studied at travel speeds of 6 and 10 mm/s.

In the first section, the flow velocity inside the weld pool is discussed. Then, a comparison is made between unstirred and stirred welds for the two travel speeds (4 and 8 mm/s), focusing on geometrical effects, weld bead appearance, porosity and effects on the welding process. In Section 5.4, a comparison is made between the grain structure for the unstirred and stirred welds. Where possible, this is related to weld pool flow and its effect on temperature gradients. The last section gives some results with regard to the influence of EMS on the hot-cracking susceptibility.

5.2. Weld pool flow velocity

Investigators have always been interested in the flow velocity inside the weld pool due to EMS. Malinowski-Brodnicka et al. [15] for instance estimated the rotational flow velocity in their experiments to be some 500 mm/s. Recently, De Vries [2] proposed a simple model to calculate the weld pool flow due to an axial magnetic field. If we use his model for a travel speed of 4 mm/s, the calculated maximum rotational flow velocity within the weld pool would be some 15 m/s. In reality, the value will be much lower due to multiple reasons.

First of all, and probably most importantly, De Vries's model does not take temperature differences within the weld pool into account. However, these account for differences in density, and - even more influential - for differences in viscosity. The viscosity towards the sides of the weld pool where a mushy zone is present can easily be a hundred times higher [27]. This will decrease the flow velocity accordingly. Secondly,

Table 2: Used welding current for different travel speeds.

Travel speed (mm/s)	4	6	8	10
Welding current (A)	148	169	199	215

his model assumes a constant magnetic field and ample time to overcome the fluids inertia. This is probably not the case for alternating EMS, again reason to expect the rotational flow to be slower. Other reasons to expect a slower velocity are the welding current distribution, the non-cylindrical shape of the weld pool and the fanning of the magnetic field.

These factors will have considerable influence on the weld pool flow velocity, diminishing its value. The flow velocity probably approaches the range of centimetres to millimetres per second, and the effects of the net rearward flow might indeed be felt, as expected by Kovalev and Rybakov [28].

5.2. General observations

5.2.1. Unstirred welds

- Weld bead appearance

The used welding currents are listed in Table 2. From this table, it can be seen that the welding current does not increase as much as the travel speed does. As the arc voltage hardly changes (because of the constant arc length), and weld penetration remains similar, this must mean an increase in process efficiency for higher travel speeds.

Particularly at low travel speed (4 mm/s), weld penetration varied considerably along the welds: about halfway down the weld length, penetration lessened to increase again towards the end. This sand-glass shape is a result of the heat flow into the plate. Initially, most of the base metal can act as a heat sink and is ahead of the arc. Heat flow in the other direction is mostly reflected from the side, resulting in good weld penetration. Approaching the middle, however, heat can flow both ahead and back, diminishing penetration. Then with increasing weld length, the plate is already heated up and the heat is reflected again, this time from the far side, causing the weld penetration to increase again. At high travel speeds, once full penetration was reached, it hardly changed over the weld length.

Adjacent to the welds, a whitened zone was found on both sides, about as wide as half the weld width. These zones are formed when the arc jumps to places with the lowest electrical resistance. The width of these whitened zones seems to decrease marginally at higher travel speeds, probably because the higher welding current makes

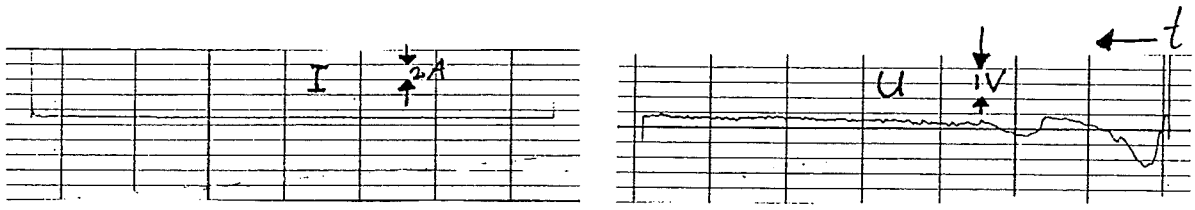

Figure 5.1 Typical graph for welding current and arc voltage for unstirred weld.

for a more rigid arc. These zones are not only unwanted because of cosmetic reasons, but also because by this jumping of the arc, heat is lost, diminishing the efficiency.

For the travel speeds used, the weld pool shape varied from purely elliptic to oval. A teardrop shape with angular backside was not found. For travel speeds from 6 mm/s upwards, the use of the alternating current became visible as very small ripples on the weld surface (AC-ripples). This is probably due to the periodical ion bombardment of the weld pool.

- Porosity

The welds exhibited a considerable degree of porosity, as a rule of thumb along the fusion boundaries. Along these boundaries, the viscosity is high, trapping gas bubbles. However, the results with regard to porosity proved very irreproducible, although all welds were made with a constant gas flow of 10 l/min. The gas bubbles generally contain trapped hydrogen, originating from water vapour from the atmosphere, oil, grease, et cetera, dissociated in the arc.

- Other remarks

During welding, the welding monitor gave a constant value for the welding current, which is controlled by the power source. The arc voltage, however, was less regular because of changes in the arc length. These result from the jumping of the arc, from the cut between the starter plate and the welding plate and from the variation in weld penetration and thereby in weld sagging. A typical graph for the welding current and for the welding voltage can be seen in Figure 5.1.

5.2.2. Stirred welds

For alternating stirring, the number of reversals of the Lorentz force per unit length is not only dependent on the stirring frequency, but also on the travel speed. Therefore, when discussing topics like numbers of ripples, it would be best to not just refer to a stirring frequency, but to a stirring quotient (SQ), which can be defined as:

$$SQ = \frac{\nu_S}{v} \tag{12}$$

with ν_S the stirring frequency (Hz) and v the travel speed (mm/s).

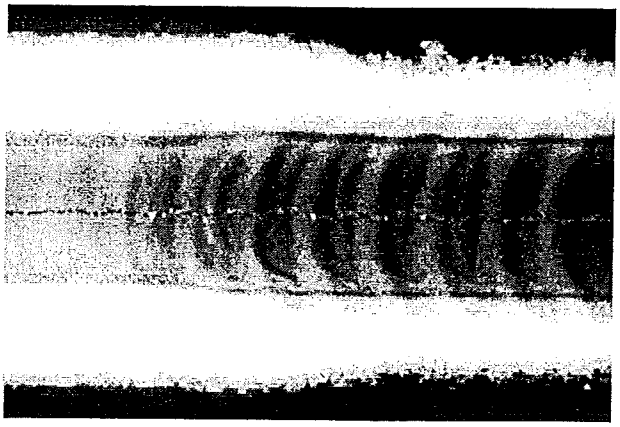

Figure 5.2 Partially stirred weld. (Travel speed = 4 mm/s, stirring frequency = 1 Hz).

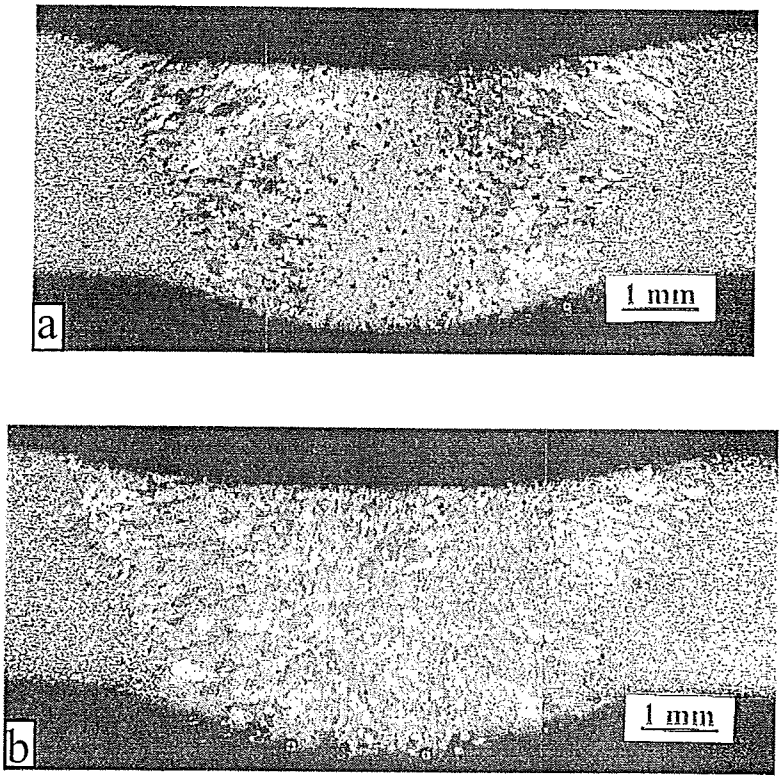

Figure 5.3 Weld cross-sections. Travel speed = 4 mm/s. a: unstirred, b: stirred at 1 Hz.

- Weld bead appearance

In Figure 5.2, a weld can be seen which has been partially stirred. On stirring, the weld width can be seen to increase, at the top, as well as the bottom side of the workpiece (Figure 5.3) . This is a result of the rotational flow in the weld pool, which broadens the weld, due to the centrifugal forces and the superheated metal, transported from the front of the weld pool, melting its way into the fusion boundary. In this way, the degree of superheat diminishes, as does the temperature gradient. The heat input no longer used for the creation of this extra superheat can then be used to melt weld metal. This causes an increase in the melting efficiency η_s, as is demonstrated below.

The melting efficiency is defined as the part of the arc energy which is at least needed to heat and melt the weld metal [3]:

$$\eta_s = \frac{qAv}{UI} \tag{13}$$

with q the heat needed to heat a unit volume of metal from room temperature to melting temperature and to melt it (J/m^3), A the cross section area of the weld bead (m^2), v the travel speed (m/s), U the arc voltage (V) and I the welding current (A). As not all the arc energy is used to melt weld metal, but also to create superheated molten metal, to heat the base metal, et cetera, the melting efficiency has a value lower than one. Now, A was found to increase due to EMS and q is a constant, then if HI stay unchanged this must have resulted from an increase in the melting efficiency, as stated above. (Another possibility, though less likely, is that HI is increased through an increase in the process efficiency η_p (cp. Equation 1), or a combination of both.) The increase in weld width and penetration is also in accordance with the fact that for very high magnetic field strengths, welds are found to burn through [21].

It can also be seen that the width of the whitened zones decreased, probably resulting from the fact that the magnetic field, which also influences the arc, allows less erratic movement to the side. For low stirring quotients, the whitened zones had curved boundaries, corresponding to the curved fusion boundaries of the weld (see below), indicating controlled sideways movement of the arc due to the magnetic field.

Due to the alternating stirring, the centreline and the fusion boundaries were no longer straight, but weaved, as during each half cycle, superheated metal from the front of the weld pool is transported along the fusion boundary on either side of the weld,

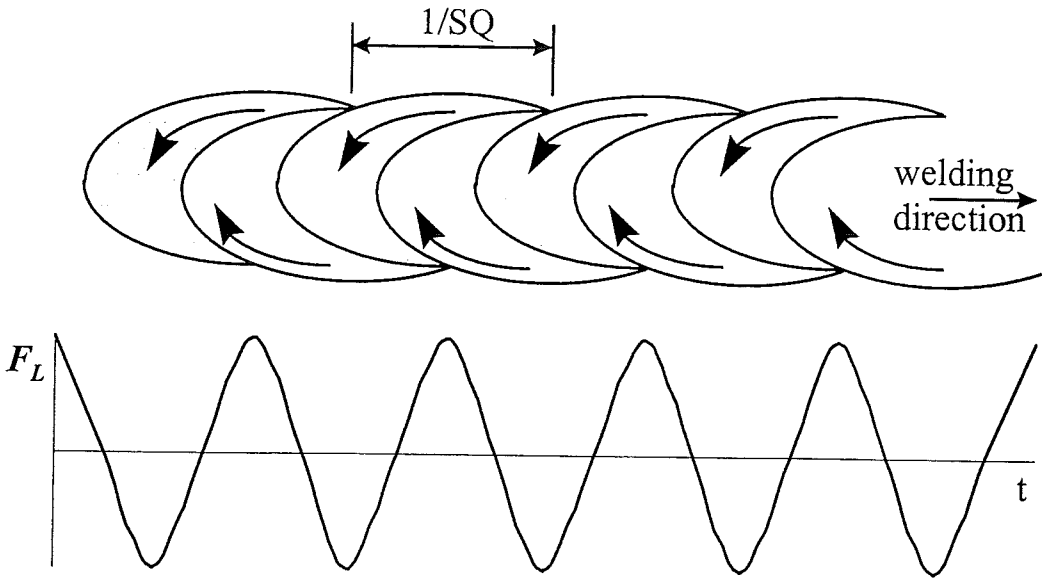

Figure 5.4 Schematic drawing of the weld bead appearance due to alternating EMS (top view) and the Lorentz force on the same distance scale.

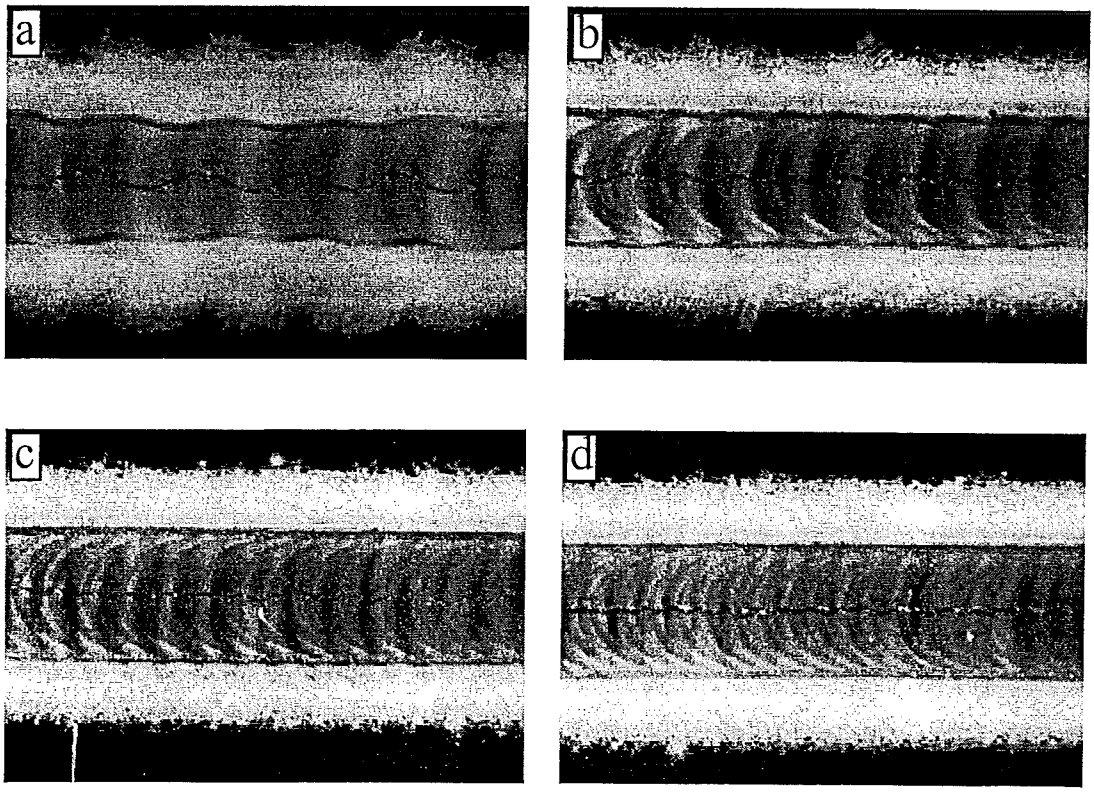

Figure 5.5 Weld bead appearance for welds stirred with different stirring quotients (travel speed = 4 mm/s). a: SQ = 0.125 mm^{-1}, b: SQ = 0.25 mm^{-1}, c: SQ = 0.375 mm^{-1}, d: SQ = 0.50 mm^{-1}.

whilst the other side is cooled-down with molten metal from the back of the weld pool, where the temperature is lowest. As a result, on the hot side, the weld pool width is extended, whilst on the cold side, the width is diminished (Figure 5.4). The weaving effect was most pronounced at low stirring quotients and diminished with increasing stirring frequencies, to disappear eventually.

The change in stirring direction also resulted in ripples on the weld surface. The orientation of the ripples for a low stirring quotient can also be seen in Figure 5.4. In this figure, it can be seen that the ripples were not symmetric with regard to the middle of the weld, due to the hot and cold side. The amount of ripples per millimetre equals twice the stirring quotient SQ, as every half cycle produces a separate ripple. With increasing SQ, the ripples became less pronounced for more than one reason. If the SQ is increased solely by increasing the frequency, this diminishes the strength of the magnetic field (cf. Chapter 4.4.), and the increase in frequency allows less time to overcome the metal's inertia. If on the other hand the SQ is increased by a decrease in the travel speed, this is accompanied by a decrease in the welding current (to maintain a comparable weld penetration). This diminishes the strength of the Lorentz force (cf. Equation 4), making the ripples less pronounced. Examples of welds made with different stirring quotients can be seen in Figure 5.5.

Close observation with the naked eye revealed the presence of very small ripples in-between the larger ripples. Although in size comparable to the AC-ripples found at higher travel speeds, they also occurred on the samples welded with a travel speed of 4 mm/s. When looking with a magnification of 25 times at these welds, the presence of small ripples on the large ripples became visible, next to the small ripples in-between the large ripples. When calculating the frequency of these ripples through the stirring quotient (Equation 12), they appear to be in the range of 50 Hz, rather than 100+ Hz. Therefore, it seems logical to conclude that these ripples are also AC-ripples. However, even when looking with a magnification of 25 times, these ripples were not seen on the unstirred welds at 4 mm/s. It is unclear why these become visible when EMS is applied.

The small AC-ripples found at higher travel speeds on unstirred welds were also found on the large ripples of the stirred welds at those travel speeds. Microscopic observation of these small AC-ripples rendered an unexpected result. The AC-ripples found on the larger ripples varied in width: the AC-ripples on the colder side were closer together than those on the hot side (Figure 5.6), contrary to expectations. This

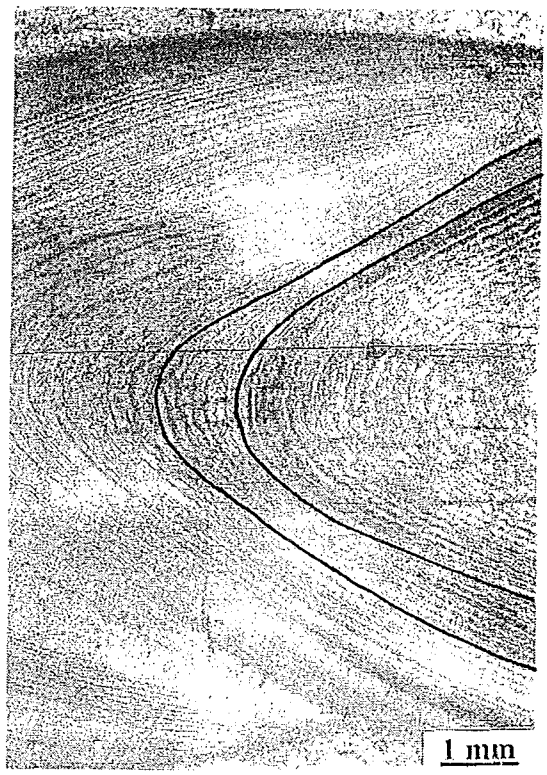

Figure 5.6 Weld pool AC-ripples in stirred weld. Travel speed = 8 mm/s. Stirring frequency = 1 Hz. Lines drawn to indicate local differences in distance between set number of AC-ripples.

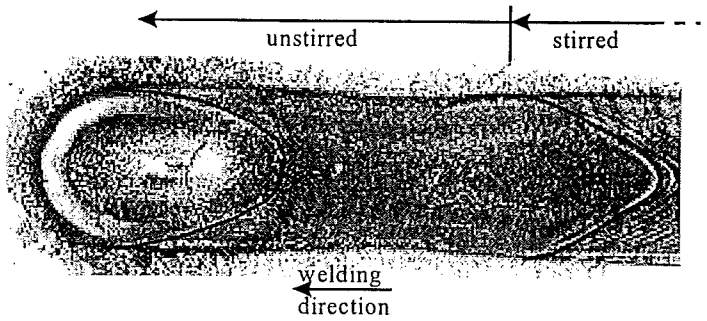

Figure 5.7 Weld pool shape in unstirred and stirred condition. Lines drawn to show weld pool shape.

would indicate that solidification there is slower than on the hot side. No explanation has yet been found, and further investigation should prove useful.

The ditch-dike effect, known to result from unidirectional stirring, was also visible after alternating stirring for moderate stirring quotients. However, for alternating stirring, the ditch and dike are weaved. As was the case for the ripples, the ditch-dike effect became less pronounced for higher stirring quotients.

In welds which have only been partially stirred, a comparison could be made between the weld pool shape for stirred and for unstirred welds. It was been found, that EMS lengthens the weld pool. However, its shape also changed, towards a teardrop shape rather than towards a round weld pool (Figure 5.7). This implies that the resultant weld pool flow is not rotational, at least not at the back of the weld pool.

There may have been different factors influencing the weld pool shape. First of all, lengthening of the weld pool indicates flattening of the temperature gradient, as may be expected. Secondly, the combination of rotational and net rearward flow might have been of influence. The total flow velocity on the hot side is the sum of the rotational flow and the net rearward flow, whilst on the cold side, it is the difference between the rotational flow and the net rearward flow. If both are of the same order of magnitude, this might have considerable influence on the weld pool shape. Thirdly, the hot fluid may melt its way into the just solidified metal at the back of the weld pool on the hot side. This leads to a small bay at the back of the pool, in which molten metal can pile up, leading to the aforementioned (weaved) ditch-dike effect. The formed pile-up hinders rotational flow along the back or the weld pool. Lastly, viscosity on the cool side is higher, obstructing weld pool flow on that side.

- Porosity

Whereas porosity in the unstirred welds was mainly found along the fusion boundaries, in the stirred welds bubbles were often found near the centre of the weld. They were generally bigger in size than those for the unstirred welds, for which there might be two reasons. Firstly, it might be that small bubbles from along the fusion boundary are swept into the weld by the weld pool flow, possibly combining small bubbles into larger ones. However, a more probable reason seems to be, that on reversal of the flow, some turbulence occurs, sometimes capturing gas in the weld pool. This might particularly be

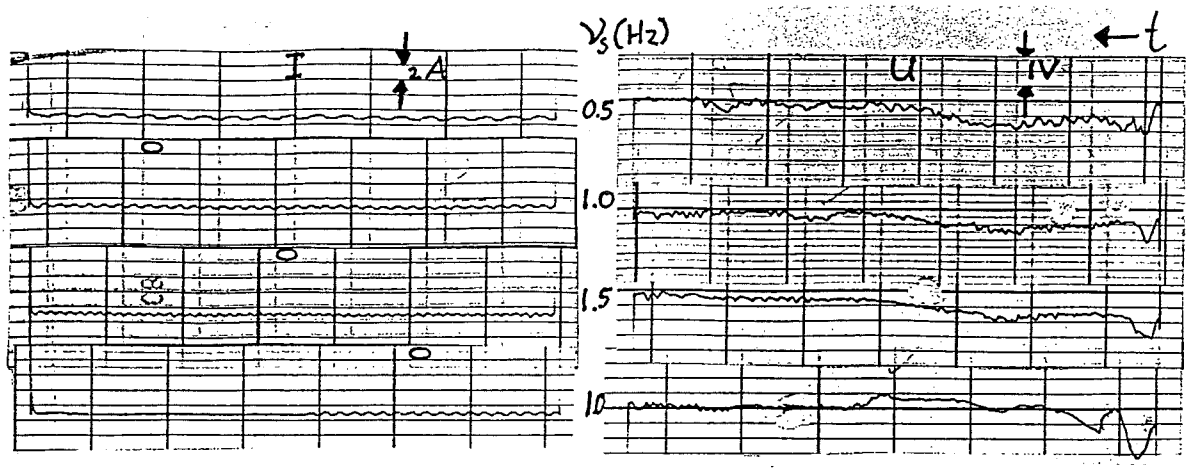

Figure 5.8 Welding current and arc voltage during stirring.

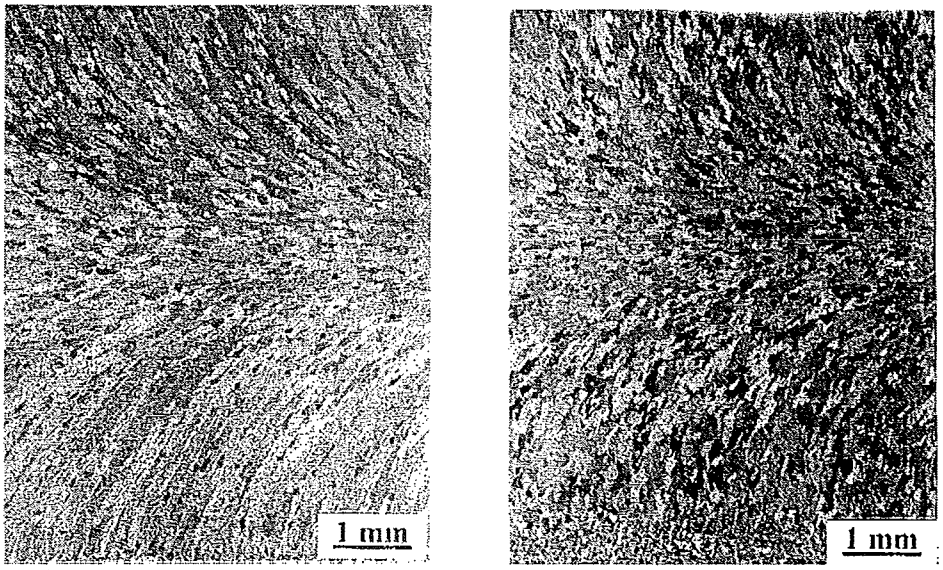

Figure 5.9 Grain structure of unstirred welds at a travel speed of 4 mm/s (top view).

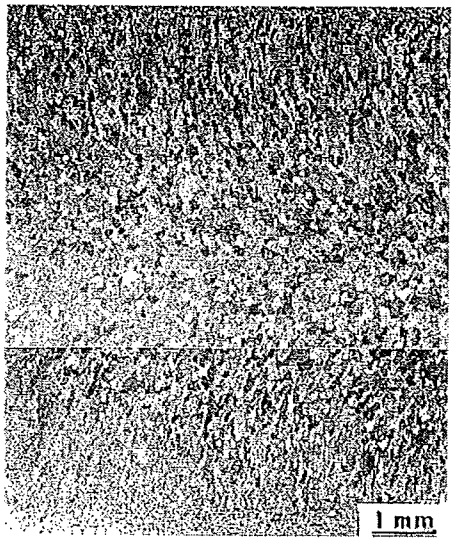

Figure 5.10 Grain structure of unstirred weld at a travel speed of 8 mm/s (top view). Compositional photograph.

the case for the larger bubbles near the weld centreline. However, further investigation is needed.

- Other remarks

During EMS, the arc jumped around in a regular manner, following the stirring frequency. Theoretically, the arc should only experience a rotational Lorentz force. However, it will be known by now that within the weld pool during each half cycle one side of the weld is heated. As the arc prefers the hottest part of the weld pool, it would then periodically change side. This explanation is also in accordance with the weaving pattern of the whitened zones. It might also be that the magnetic field is not completely homogeneously axial, but on calibration, no proof for this hypothesis has been found.

From a graph showing the welding current and arc voltage (Figure 5.8), it can be seen that the welding current became a sinusoidal wave-form due to the changing resistance of the arc (as the welding current is resistance controlled). This change in welding current was almost only noticeable at low travel speeds. The arc voltage also changed, due to the jumping of the arc and the resultant change in its length.

5.3. Grain structure

To examine the grain structure without interference of hot cracks, welds have been made on uncut plates. Close examination of the grain structure has been performed for two travel speeds: 4 mm/s and 8 mm/s. It was found that difference in welding current between partial weld penetration and full weld penetration is very small, in the order of a few amperes. (This was also found for welding aluminium alloys of different chemical composition [29].) Next to this, sagging of the weld occurred even before complete weld penetration was reached, that is before the metal has been molten down to the bottom of the weld. Furthermore, the welds proved very sensitive to all kinds of influences, such as small variations in welding current, in surface quality and in waiting time at the beginning. All these effects do not contribute to the reproducibility of the experiments. Although no direct proof has been found, this might also mean that strictly speaking welds made on uncut plates cannot be compared with welds made with similar settings on cut plates.

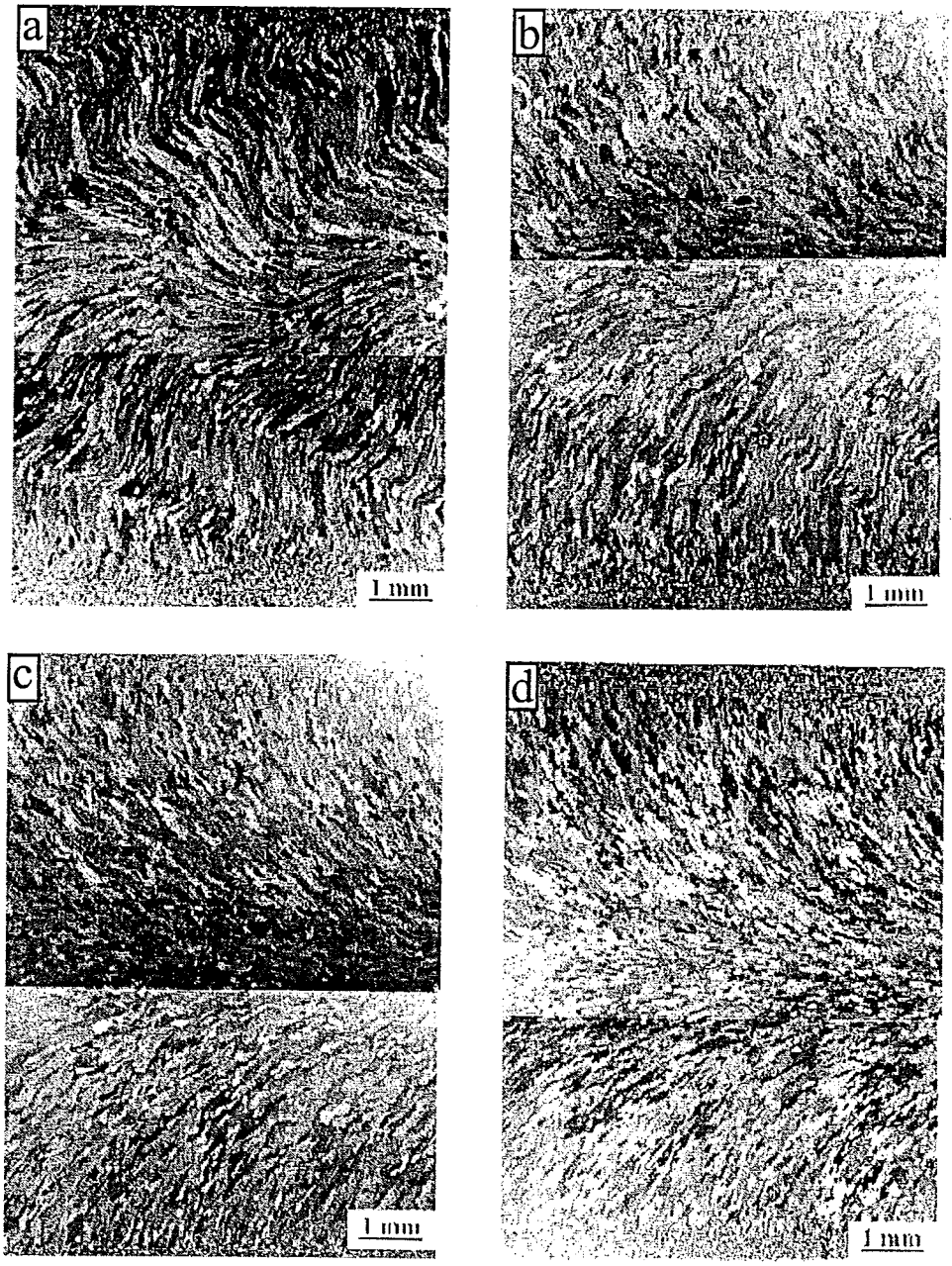

Figure 5.11 Grain structure of stirred welds at a travel speed of 4 mm/s (top view). a: ν_s = 1 Hz, b: ν_s = 2 Hz, c: ν_s = 5 Hz, d: ν_s = 10 Hz. Compositional photographs.

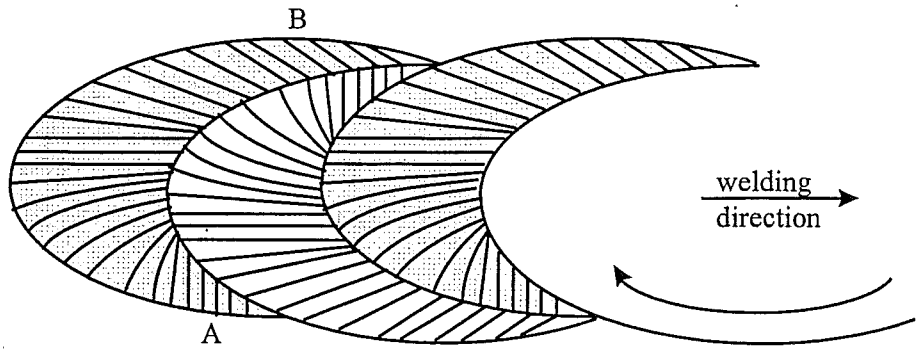

Figure 5.12 Schematic drawing of the grain structure due to alternating EMS (top view).

5.3.1. Unstirred welds

At a travel speed of 4 mm/s, the weld pool was elliptic in shape. This shape results in a constantly changing maximum thermal gradient when going from the fusion boundary towards the weld centreline (cf. Section 2.5). This results in the bent and refined structure shown in Figure 5.9. This figure shows the grain structure just underneath the surface of two welds made at the same settings. It can be seen that, although the same welding current, welding speed, et cetera, have been used, the structures differ considerably. But then it is known that in welding aluminium, many parameters are of influence, as mentioned above.

At a travel speed of 8 mm/s, the weld pool shape was more oval. According to Section 2.5, due to the higher travel speed and therefore lower value for the G/R ratio more small (equiaxed) grains might be expected. As can be seen in Figure 5.10, this was indeed found: the columnar grains present tend to be smaller in size (i.e. shorter). At this speed, less variation was found in the grain structure of the different welds made with the same settings.

5.3.2. Stirred welds

Also in the case of stirred welds was the grain structure examined at 4 and 8 mm/s. EMS has been applied at four frequencies: 1, 2, 5 and 10 Hz.

The grain structure just below the surface at 4 mm/s can be seen for the used stirring frequencies in Figure 5.11. Particularly in the first picture, the effect of the stirring is clear. Different sickle-shaped zones each consisting of columnar grains can be distinguished, corresponding to the ripples on the surface. Not all columnar grains are orientated perpendicular to the boundary of the ripple, some are at an angle, indicating changes in the temperature gradient due to weld pool flow. Furthermore, the orientation alternates from ripple to ripple (as of course did the flow direction). Now let us look more closely at the orientation of the grains within one ripple, as it gives an indication of the temperature gradients in the weld pool, and thereby of the weld pool flow.

The grain structure is schematically drawn in Figure 5.12. On the cold side (A), the formed grains are perpendicular to the welding direction. This is not only the case directly next to the fusion boundary, but up to about one quarter of the weld width.

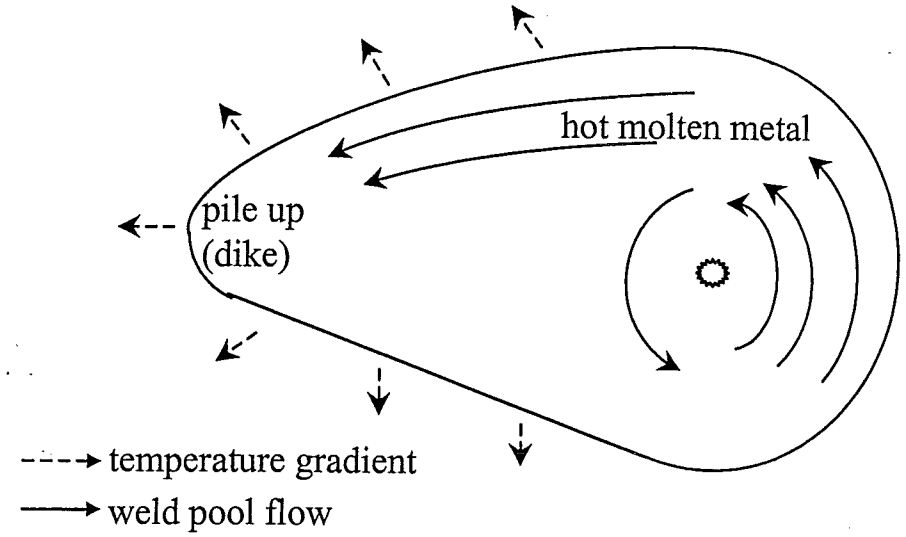

Figure 5.13 Assumed weld pool flow and resultant temperature gradients in the case of EMS.

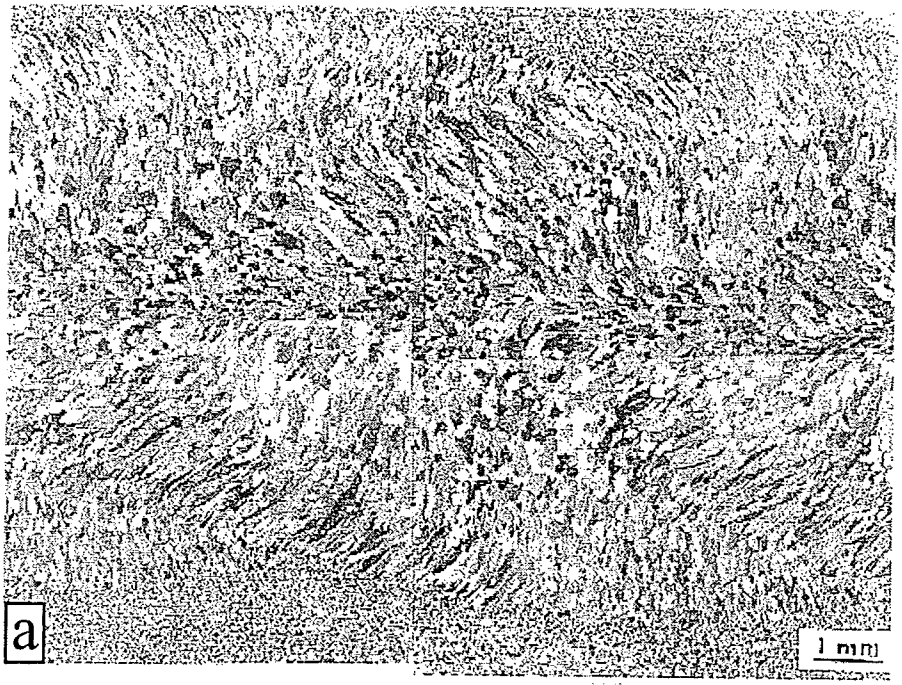

Figure 5.14 Grain structure of stirred welds at a travel speed of 8 mm/s (top view). a: ν_s = 1 Hz, b: ν_s = 2 Hz, c: ν_s = 5 Hz, d: ν_s = 10 Hz. Compositional photographs.

Apparently, the steepest temperature gradient no longer points in the direction of the arc, but merely to the other side of the weld. Therefore, it might be concluded, that the hot fluid from the front of the weld pool is still of considerable temperature when it reaches the back of the weld pool. As a result, the grains on the cold side grow in the direction of the hot side, perpendicular to the welding direction. On the hot side (B), the grains are orientated more in the welding direction, as there is still a temperature gradient present along the flow direction. The assumed weld pool flow and resultant temperature gradients are schematically drawn in Figure 5.13. However, further investigation is needed to find out the exact flow pattern and orientation of the temperature gradients.

The applied EMS can result in refined grains, but apparently only by blocking-off columnar grains. Whether or not grain refinement occurs is then very much dependent on the unstirred grain structure. However, this grain structure proved very irreproducible, so a clear statement cannot be made. It might even be that application of EMS with a low SQ can deteriorate the grain structure of the weld by introducing large columnar grains. What is clear, however, is that maximum effect will then be reached when the SQ is chosen in such a way, that the length over which columnar grains can grow is about as long as the grains are wide. This calls for a frequency of some 10 Hz (SQ = 2.5 mm^{-1}). However, at this SQ, sickles in the grain structure are no longer visible, due to the high frequency used. Furthermore, at high travel speeds, the high frequency needed may be too high to be effective.

No evidence was found for the occurrence of dendrite fragmentation. Grain detachment seems more probable, as small grains have been found at the ripple boundaries, particularly near the fusion boundary along which the hottest metal was transported. These small grains may have originated from the mushy zone.

At a travel speed of 8 mm/s, similar effects occurred (Figure 5.14). However, due to the higher travel speed, the columnar bands are separated by zones with equiaxed grains. This might be due to the increased influence of the periods of inertia, as the travel speed is higher or to the increased influence of the (higher) net rearward flow. More research is needed on this subject. As the unstirred grain structure at this speed was already more refined than in the case of a travel speed of 4 mm/s, EMS can be said to lead to a deterioration of the grains structure.

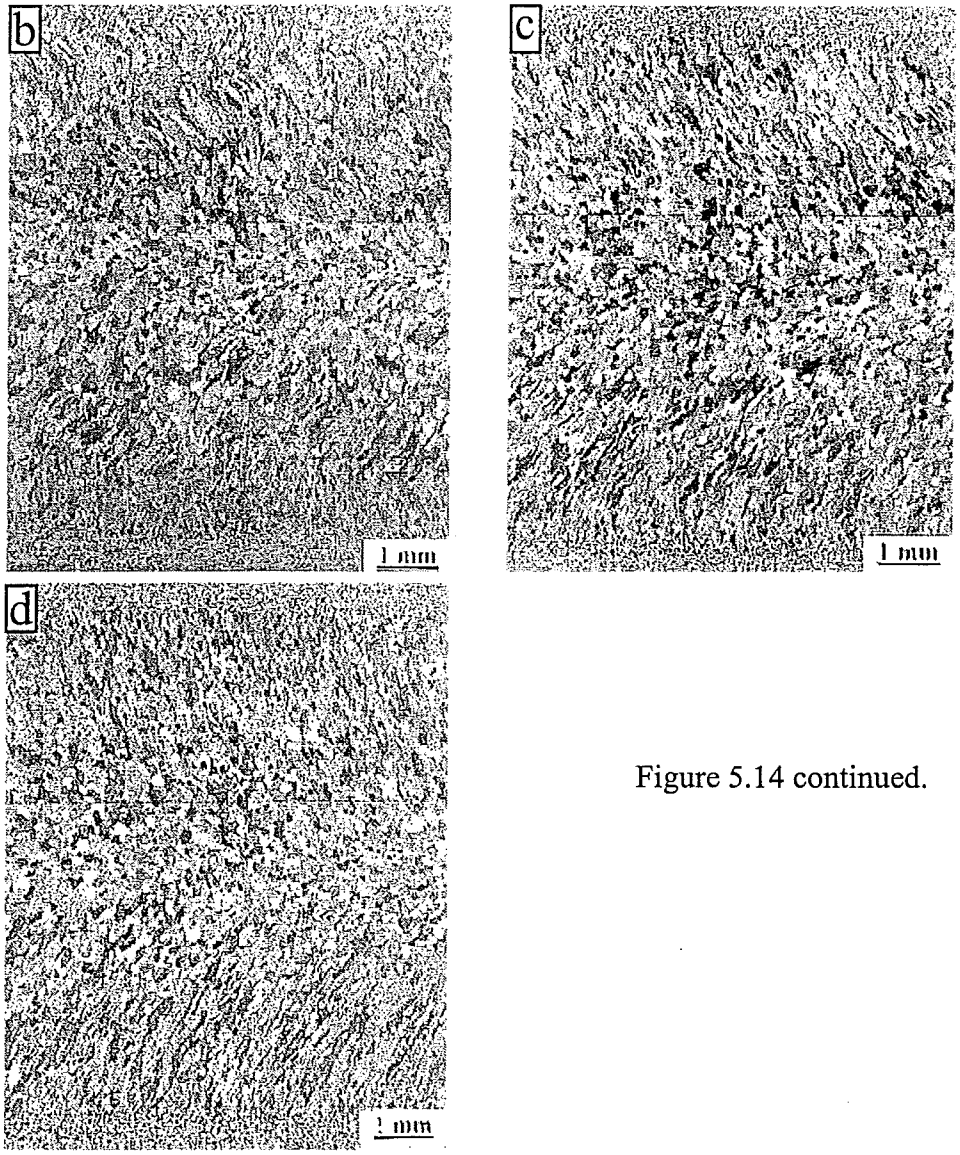

Figure 5.14 continued.

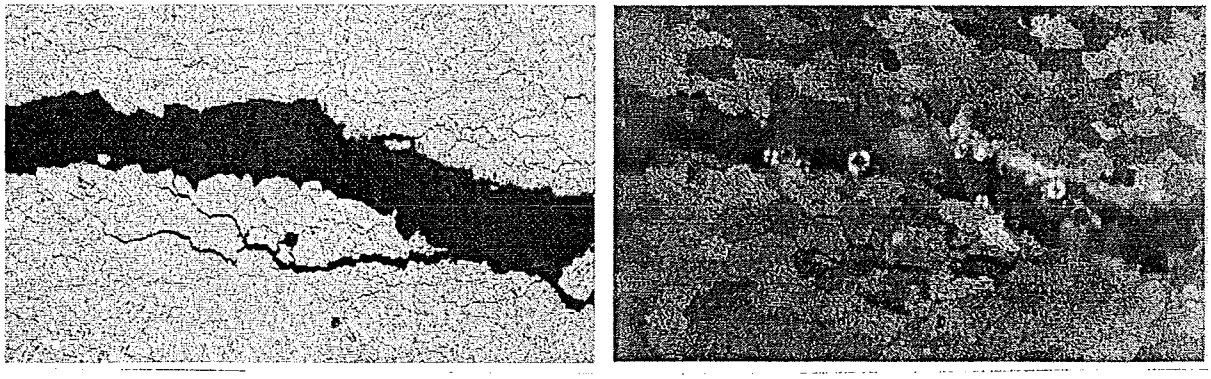

Figure 5.15 Grain structure around a hot crack (top view) in an unstirred weld using ordinary light microscopy and using polarised light microscopy (63x).

5.4. Hot cracks

The research on this subject might be seen as preliminary. Further research, particularly with quantitative tests like the Houldcroft test, is needed.

5.4.1. Unstirred welds

At all travel speeds (4, 6, 8 & 10 mm/s), the welds were found to crack along the centreline plane over the entire length of the weld on the welding plate. The cracks had a considerable opening just after welding (due to the thermal expansion of the base metal). This opening was larger at smaller travel speeds, due to the fact that at these travel speeds total welding time is longer and efficiency is worse. Therefore, more heat flows into the base metal, thus causing it to expand more. Furthermore, in all cases, small crater cracks were found at the end of the weld. Because welds on uncut plates did not crack, except for small cracks in the crater at the end of the weld, the expansion of the base metal was probably the most influential reason for the cracking of the welds.

Using (polarised) light microscopy, it was found that the cracks indeed run intergranularly, as was expected. This can be seen in Figure 5.15, showing two pictures of the same part of a centreline crack, one using ordinary bright field light microscopy and one using polarised light microscopy (to show the separate grains). It can also be seen, particularly in the non-polarised light picture, that around the major crack, small cracks are present. This indicates that cracking takes place in two stages. First, small micro-cracks are formed, when the stress on the network of primary dendrites rises. Then, a big crack starts to grow, connecting smaller cracks. This causes such stress relief, that the smaller cracks stop growing. This process of centreline cracking is similar to that found in direct chilled continuous casting [30]. As the cracks are still open, it is obvious that no eutectic healing takes place.

5.4.2. Stirred welds

Although EMS was used, the welds were still found to crack, although in a somewhat different pattern than the unstirred welds. As can be seen in Figure 5.16, the crack was

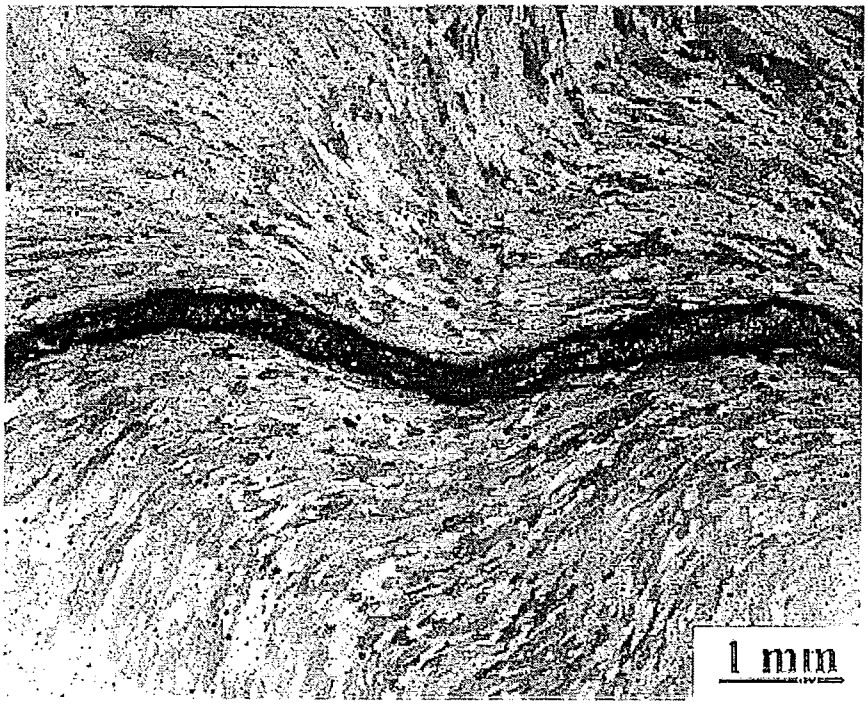

Figure 5.16 Grain structure around a hot crack (top view) in a stirred weld using ordinary light microscopy and polarised light microscopy. Travel speed = 4 mm/s. Stirring frequency = 1 Hz.

again intergranular. Although it followed a weaved path, the dissipation of energy due to the weaving pattern proved too little to stop the crack.

Only a few welds were made on Houldcroft specimens, as preliminary testing. Welds were made at 4 mm/s, without EMS and with EMS with a stirring frequency of 1 Hz. At both settings, two welds were made. One unstirred weld and one stirred weld still cracked over the entire length, whereas the cracks in the other unstirred and stirred weld arrested at 1.5 cm and 1 cm before the end of the weld, respectively. This indicates that no great improvement in the hot-cracking susceptibility is to be expected to occur just from weaving of the centreline.

6. Conclusions and recommendations

6.1. Conclusions

On the basis of the results obtained in this project, the following conclusions can be drawn:

1. Welding of AA 6082 aluminium-magnesium-silicon alloy calls for very close control of all parameters, such as welding current, surface quality, flatness of the plate, et cetera.
2. The transition between partial and full weld penetration depends critically on the welding current. A difference of 1 or 2 amperes in welding current makes a considerable difference in weld penetration.
3. Low-frequency Electro-Magnetic Stirring (EMS) can effectively be applied during AC TIG welding. The frequency of the magnetic field should then be the desired stirring frequency plus the frequency of the welding current.
4. Alternating EMS changes the shape of the weld pool towards a shape an unstirred weld pool would have at higher travel speeds.
5. In the case of AA6082, grain refinement takes place through changing the orientation of the temperature gradients. This calls for high stirring quotients, diminishing the effect of EMS.
6. Grain refinement only is useful in the case in which the unstirred grain structure is columnar in nature. This is the case at low travel speeds.
7. No solid evidence for grain detachment or dendrite fragmentation has been found.
8. Alternating EMS can introduce large gas bubbles in the weld.
9. The preliminary hot-cracking tests revealed no improved resistance to hot cracking in the case of stirred welds.

6.2. Recommendations

To study the effect of EMS in more detail, it is useful to return to the basics. Further research might therefore aim at:

- Gaining more knowledge of the exact flow patterns within the weld pool. For this purpose, tracer technology might prove useful, or controlled addition of filler material, not necessarily aluminium.
- Gaining more knowledge of the exact influence of EMS on the temperature gradients within the weld pool. For instance, what temperature has the superheated liquid from the front of the weld pool by the time it reaches the back? Placing thermocouples at different locations and heights in the weld pool might prove useful.
- Making a study of the influence of this kind of EMS on the formation or prevention of weld porosity. For this purpose, a shielding gas with some added H_2 might be used, as this will increase the degree of porosity.
- Making a comparison between EMS during DC TIG welding and EMS during AC TIG welding. This might for instance show if the high-frequency components really are too fast for the weld pool flow to follow.
- Investigating the influence of the wave-form for the Lorentz force.
- Investigating the influence of EMS on the local solidification rate. This can for instance be performed through close observation of the AC-ripples.

References

[1] C.H.J. Gerritsen,
The Influence of External Magnetic Fields on the Gas Tungsten Arc Welding Process and on the Weld Properties. A Literature Review.
TU Delft, Delft, January 1998.

[2] H.W. de Vries,
Weldability of Aluminium-Matrix Composites,
Ph.D.-thesis, Delft University Press, Delft, 1998.
ISBN 90-407-1791-5.

[3] G. den Ouden,
Lastechnologie.
Delftse Uitgevers Maatschappij, Delft, Second printing, 1990.
ISBN 90-6562-087-7.

[4] H.W. Kerr,
Solidification and grain structures in welds.
In: International trends in welding science and technology. Proceedings of the 3rd Intern. Conf. on Trends in Welding Research,
Gatlinburg (U.S.A.), June 1-5, 1992, 157-166.

[5] D.A. Porter and K.E. Easterling,
Phase Transformations in metals and alloys.
Chapman & Hall, reprint 1991.
ISBN 0-412-38400-0.

[6] A. Matsunawa,
Modeling of heat and fluid flow in arc welding.
In: International trends in welding science and technology. Proceedings of the 3rd Intern. Conf. on Trends in Welding Research,
Gatlinburg (U.S.A.), June 1-5, 1992, 3-16.

[7] R.A. Willgoss,
A practical future for em stirring of the weld pool?
Welding and Metal Fabrication, May (1981), 189-197.

[8] S. Kou,
Grain structure development in the fusion zone.

In: Recent trends in welding science and technology. Proceedings of the 2nd Intern. Conf. on Recent Trends in Welding Science and Technology,
Gatlinburg (U.S.A.), May 14-18, 1989, 137-146.

[9] Y. Le and S. Kou,
Formation of three types of new grains in the weld metal.
In: Advances in Welding Science and Technology. Proceedings of an Intern. Conf. on Trends in Welding Research,
Gatlinburg (U.S.A.), May 18-22, 1986, 139-144.

[10] S. Kou and Y. Le,
Alternating grain orientation and weld solidification cracking.
Metallurgical Transactions A, 16A 10 (1985), 1887-1896.

[11] B.T.J. Stoop,
De invloed van een aantal lasparameters op de stolstructuur van TIG-gelaste aluminiumlegeringen.
Master's Thesis, Delft University of Technology, November 1985.

[12] J.C. Villafuerte and H.W. Kerr,
Electromagnetic stirring and grain refinement in stainless steel GTA welds.
Welding Journal, 69 1 (1990), 1s-13s.

[13] Sindou Kou,
Welding metallurgy.
John Wiley & Sons, 1987.
ISBN 0-471-84090-4.

[14] D.C. Brown, F.A. Crossley, J.F. Rudy and H. Schwartzbart,
The effect of electromagnetic stirring and mechanical vibration on arc welds.
Welding Journal, 41 6 (1962), 241s-250s.

[15] M. Malinowski-Brodnicka, G. den Ouden and W.J.P. Vink,
Effect of electromagnetic stirring on GTA welds in austenitic stainless steel.
Welding Research, 69 2 (1990), 52s-59s.

[16] D.R. Poirier and G.H. Geiger
Transport phenomena in materials processing.
TMS, Warrendale, Pennsylvania (U.S.A.), February 1994.
ISBN 0-87339-272-8.

[17] William E. Boyce and Richard C. DiPrima,
Elementary differential equations and boundary value problems.

John Wiley & Sons, Inc., fifth edition, 1992.
ISBN 0-471-57019-2

[18] T. Watanabe, H. Nakamura and K. Ei,
Solidification control of austenitic stainless steel weld metal by electromagnetic stirring.
Transactions of the Japan Welding Society, 21 2 (1990), 37-43.

[19] W.J.P. Vink, M. Malinowski-Brodnicka and G. den Ouden,
Invloed van elektromagnetisch roeren op eigenschappen van lasverbindingen in roestvast staal.
Lastechniek, 54 (1988), 105-109.

[20] M.A. Abralov and R.U. Abdurakhmanov,
Mechanism by which electromagnetic action breaks down primary structure of weld metal.
Automatic Welding, 35 2 (1982), 14-17.

[21] F. Matsuda, H. Nakagawa, K. Nakata and R. Ayani,
Effect of electromagnetic stirring on weld solidification structure of aluminium alloys (Report I). Investigation on GTA weld metal of thin sheet.
Transactions of JWRI, 7 1 (1978), 111-127.

[22] F. Matsuda, K. Nakata and N. Sano,
Effect of electromagnetic stirring on weld solidification structure of austenitic stainless steels.
Transactions of JWRI, 15 2 (1986), 155-166.

[23] B.P. Pearce and H.W. Kerr,
Grain refinement in magnetically stirred GTA welds of aluminum alloys.
Metallurgical transactions B, 12B (1981), 479-486.

[24] C. Jia and K. Xiao,
Improvement of weld qualitiy by electromagnetic stirring of the weld pool.
In: Proceedings Eighth Intern. Conf. on Offshore Mechanics and Arctic Engineering,
The Hague (NL), March 19-23, 1989, 117-120.

[25] P.T. Houldcroft, B.Sc.,
A simple cracking test for use with argon-arc welding.
British Welding Journal, 2 10 (1955), 471-475.

[26] L.J. Barker,

Revealing the grain structure of common aluminum alloy metallographic specimens.
Transactions of the ASM, 42 (1950), 347-356.

[27] C.J. Quaak,
Rheology of partially solidified aluminium alloys and composites.
Ph.D.-thesis, Eburon P&L, Delft, 1996.
ISBN 90-5651-019-3.

[28] I.M. Kovalev and A.S. Rybakov,
The movement of liquid metal in the weld pool in welding in a longitudinal magnetic field.
Automatic Welding, 30 9 (1977), 38-40.

[29] R.G.G.M. Pieters and T. Luijendijk,
Onderdeel A1 Het lassen van aluminium legeringen met verschillende chemische samenstelling (vervolg op bijlage 1 onderdeel 1-1 van document LA94-15).
Technische Universiteit Delft, December 1994.

[30] M.E. Pieterse,
Hot cracking of aluminium magnesium and aluminium-magnesium-silicon alloys during D.C.casting.
Master's Thesis, Delft University of Technology, August 1998.